Stem Cell Reports
Article

ISSCR

OPEN ACCESS

WNT7A suppresses adipogenesis of skeletal muscle mesenchymal stem cells and fatty infiltration through the alternative Wnt-Rho-YAP/TAZ signaling axis

Chengcheng Fu,[1] Britney Chin-Young,[1] GaYoung Park,[1] Mariana Guzmán-Seda,[1,2] Damien Laudier,[1] and Woojin M. Han[1,3,*]

[1]Department of Orthopaedics, Icahn School of Medicine at Mount Sinai, New York, NY, USA
[2]Department of Biomedical Engineering, Polytechnic University of Puerto Rico, San Juan, PR, USA
[3]Black Family Stem Cell Institute, Icahn School of Medicine at Mount Sinai, New York, NY, USA
*Correspondence: woojin.han@mssm.edu
https://doi.org/10.1016/j.stemcr.2023.03.001

SUMMARY

Intramuscular fatty infiltration in muscle injuries and diseases, caused by aberrant adipogenesis of fibro-adipogenic progenitors, negatively impacts function. Intramuscular delivery of wingless-type MMTV integration site family 7a (WNT7A) offers a promising strategy to stimulate muscle regeneration, but its effects on adipogenic conversion of fibro-adipogenic progenitors remain unknown. Here, we show that WNT7A decreases adipogenesis of fibro-adipogenic progenitors (FAPs) by inducing nuclear localization of Yes-associated protein (YAP) through Rho in a β-CATENIN-independent manner and by promoting nuclear retention of YAP and transcriptional co-activator with PDZ-binding motif (TAZ) in differentiating FAPs. Furthermore, intramuscular injection of WNT7A *in vivo* effectively suppresses fatty infiltration in mice following glycerol-induced injury. Our results collectively suggest WNT7A as a potential protein-based therapeutic for diminishing adipogenesis of FAPs and intramuscular fatty infiltration in pathological muscle injuries or diseases.

INTRODUCTION

Persistent fatty infiltration, known as myosteatosis, is a common hallmark of chronic skeletal muscle injuries and diseases that negatively impacts function and poses significant health and socioeconomic burden (Minagawa et al., 2013; Yamamoto et al., 2010). For example, in rotator cuff tendon injuries, irreversible fatty infiltration is prevalent in the associated muscles, which directly increases muscle dysfunction and retear rates following surgical repair (Fu et al., 2021; Gladstone et al., 2007; Park et al., 2015b). In muscular dystrophies, pervasive intramuscular fatty infiltration positively correlates with the disease severity (Li et al., 2015). Fatty infiltration is also common in the paraspinal and neck muscles of astronauts following spaceflights (Burkhart et al., 2019; McNamara et al., 2019). Recent evidence suggests that fibro-adipogenic progenitors (FAPs), a population of muscle-resident mesenchymal stem/stromal cells, are the primary cellular culprit that generates intramuscular fatty infiltration (Joe et al., 2010; Liu et al., 2016; Uezumi et al., 2010; Wosczyna et al., 2012). Although this link between FAPs and fatty infiltration is established, therapies that limit such pathologic fatty infiltration without compromising myogenesis currently do not exist.

FAPs play a critical role in muscle regeneration by secreting paracrine factors that promote activation and expansion of muscle stem/satellite cells (Joe et al., 2010; Uezumi et al., 2010; Wosczyna et al., 2012, 2019). Furthermore, skeletal muscles with depleted FAPs not only exhibit significantly impaired muscle regeneration but also lead to muscle atrophy under homeostatic conditions, highlighting the importance of FAPs in muscle maintenance (Wosczyna et al., 2019). Upon muscle injury, immune cells initially infiltrate the injured space to remove debris and activate both FAPs and satellite cells (Butterfield et al., 2006; Heredia et al., 2013; Tidball and Villalta, 2010). As the inflammation resolves, tumor necrosis factor α (TNF-α) released by macrophages induces apoptotic clearances of FAPs, while activated satellite cells continue to undergo myogenesis (Lemos et al., 2015). In chronic muscle pathology, however, FAPs undergo unchecked proliferation and give rise to adipocytes and myofibroblasts (Lemos et al., 2015). The resulting fatty infiltration and fibrosis perturb the highly aligned and organized muscle structure and consequently reduce the ability of muscles to contract and regenerate. Thus, identifying molecular mechanisms that regulate the adipogenic conversion of FAPs is critical for establishing strategies to combat pathologic fatty infiltration.

Intramuscular delivery of wingless-type MMTV integration site family 7a (WNT7A) offers a promising strategy to both stimulate muscle regeneration and prevent muscle degeneration (Han et al., 2019; von Maltzahn et al., 2012, 2013; Schmidt et al., 2020). WNT7A promotes myofiber hypertrophy through the non-canonical AKT/mTOR pathway and increases the symmetric expansion of muscle satellite cells through the non-canonical planar cell polarity pathway (Le Grand et al., 2009; von Maltzahn et al., 2011). In preclinical models of Duchenne muscular

dystrophy, WNT7A administration significantly increases satellite cell quantity, myofiber hypertrophy, and muscle strength (von Maltzahn et al., 2012). Controlled delivery of WNT7A using a bioengineered hydrogel also increases satellite cell quantity and myofiber hypertrophy, presenting WNT7A as an effective therapeutic candidate for treating various acute and degenerative muscle conditions (Han et al., 2019). While the past findings collectively corroborate that WNT7A can be used as a potential pro-myogenic therapeutic, the effect of WNT7A on FAPs, and specifically whether it limits adipogenic conversion of FAPs, remains unknown.

The objective of this study was to determine the mechanistic effect of WNT7A on FAPs adipogenic conversion. By using freshly isolated primary murine FAPs, we demonstrate that WNT7A effectively decreases the adipogenic potential of FAPs. We show that while WNT7A does not directly increase nuclear localization of β-CATENIN, it does induce nuclear localization of Yes-associated protein (YAP) through Rho and promotes nuclear retention of YAP and transcriptional co-activator with PDZ-binding motif (TAZ) in differentiating FAPs. We additionally show that WNT7A suppresses intramuscular fatty infiltration following glycerol injury without negatively impacting myogenesis or causing fibrosis *in vivo*. Collectively, we provide mechanistic evidence that WNT7A effectively reduces adipogenesis of FAPs and intramuscular fatty infiltration.

RESULTS

WNT7A decreases adipogenesis of FAPs

To evaluate the effect of WNT7A on lineage specification of differentiating FAPs, we carried out a series of *in vitro* experiments using primary murine FAPs. Primary FAPs ($CD31^-$, $CD45^-$, $ITGA7^-$, $SCA1^+$) were isolated from the hindlimb muscles of C57Bl6/J mice using previously reported methods (Figure S1A) (Marinkovic et al., 2019). Freshly isolated FAPs express PDGFRα (80.4% ± 4.8%; Figure S1B), a defining marker of murine FAPs (Joe et al., 2010; Uezumi et al., 2010). Primary FAPs differentiated into myofibroblasts characterized by stress fibers expressing α-smooth muscle actin (αSMA) when maintained in fibrogenic differentiation medium (FM) for 4 days (Figures S1C and S1D; $p < 0.001$), but when maintained in adipogenic differentiation medium (ADM) for 4 days, FAPs differentiated into oil red O $(ORO)^+$/$PLIN1^+$ adipocytes (Figures S1C–S1F; $p < 0.001$). Collectively, these results confirm the functional identity of the isolated primary FAPs to be used in the subsequent experiments.

To determine the dose-dependent effect of WNT7A on the adipogenic potential of FAPs, we seeded freshly isolated FAPs in a dish and let the cells proliferate to near confluency for 4 days in growth media. Proliferating FAPs were further maintained in growth medium (GM ± WNT7A) or ADM (ADM ± WNT7A) for an additional 3–4 days (Figure 1A). Note, in GM, the FAPs begin to spontaneously differentiate into both myofibroblasts and adipocytes (Joe et al., 2010). In both GM and ADM, WNT7A decreased adipogenesis in a dose-dependent manner (Figures 1B and 1C). The dose of 200 ng/mL significantly reduced the formation of ORO^+ adipocytes compared with the control (0 ng/mL; Figures 1B and 1C; $p < 0.01$). Based on this, we chose to use 200 ng/mL for the subsequent *in vitro* experiments.

To further validate the effect of WNT7A on the suppression of FAPs adipogenesis, we cultured freshly isolated FAPs to near confluency and subsequently maintained the cells in either GM or ADM, with or without 200 ng/mL WNT7A (Figure 1A). Note, the dH_2O vehicle for WNT7A (0.2% v/v in media) does not affect FAP adipogenesis (Figure S2). WNT7A significantly reduced the formation of PLIN1+ (perilipin; lipid droplet-associated protein) adipocytes (Figures 1D and 1E; $p < 0.0001$) as well as nuclear activation of PPARγ, a master regulator of adipogenesis, compared with the control (Figures 1F and 1G; $p < 0.01$). In the adipogenic condition, WNT7A also reduced PLIN1 and PPARγ expressions to below the mean of spontaneously differentiating condition (GM; Figures 1D–1G). These results demonstrate that WNT7A effectively decreases the adipogenic potential of FAPs.

We next quantified the number of cells expressing αSMA^+ stress fibers, a hallmark of activated myofibroblasts (Goffin et al., 2006; Hinz, 2007), to determine if WNT7A increases fibrogenesis in the adipogenic condition. We observed that $PLIN1^-$ FAPs in ADM with or without WNT7A treatment exhibited a base level of diffuse αSMA, but only in the fibrogenic (FM) and spontaneously differentiating (GM) conditions did the FAPs differentiate into myofibroblasts, exhibiting structurally apparent αSMA^+ stress fibers (Figures S3A and S3B). In ADM with or without WNT7A treatment, significantly fewer αSMA stress fibers-expressing myofibroblasts formed (Figures S3A and S3B; $p < 0.0001$). This suggests that WNT7A does not promote fibrogenesis in adipogenic culture conditions *in vitro*. WNT7A treatment also did not affect cell viability and proliferation (Figures S3C, S3D, and S4). Altogether, these results demonstrate that WNT7A dampens adipogenesis of FAPs without promoting fibrogenesis in adipogenic conditions *in vitro*.

WNT7A reduces adipogenesis of FAPs in a β-CATENIN-independent manner

The canonical Wnt signaling inhibits adipogenesis through suppression of the adipogenic transcription factor PPARγ in preadipocytes, marrow-derived mesenchymal stromal cells, and muscle FAPs (Bennett et al., 2002; Kang

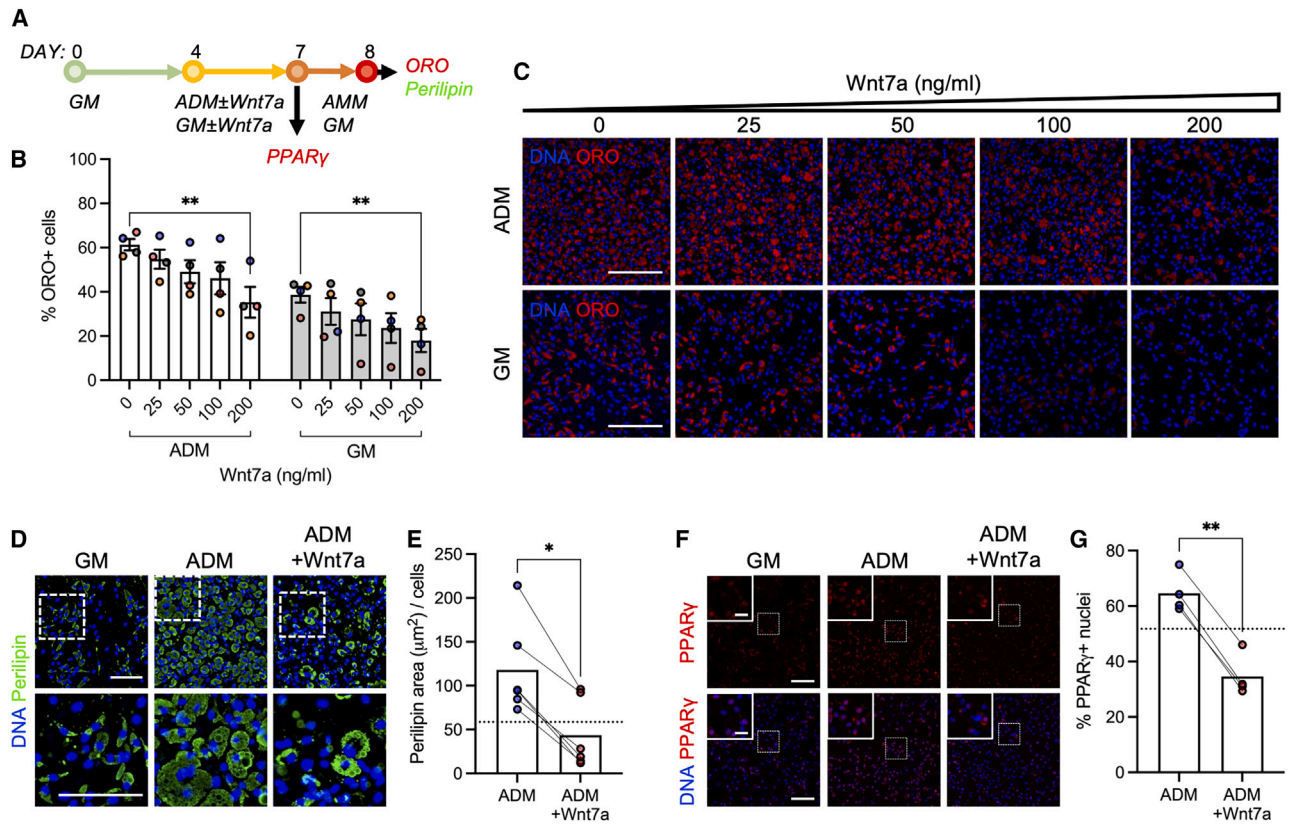

Figure 1. WNT7A decreases FAP adipogenesis

(A) Experimental timeline. GM, growth media; ADM, adipogenic differentiation media; AMM, adipogenic maintenance media.

(B) Percentage of ORO$^+$ cells treated with varying doses of WNT7A. Two-way ANOVA with Bonferroni post-hoc analyses. Mean ± SEM. Dose effect $p = 0.0021$. Media effect $p < 0.0001$. $^{**}p < 0.01$. $n = 4$. Colors represent biological replicates.

(C) Representative images of ORO-labeled cells treated with varying doses of WNT7A. Scale bar: 100 μm.

(D) Representative immunofluorescence images of perilipin-labeled FAPs cultured in GM and ADM ± WNT7A (200 ng/mL). Scale bar: 100 μm.

(E) Perilipin area normalized by cell quantity. Two-tailed unpaired t test. $^*p < 0.05$. $n = 6$. Dotted line: mean of GM.

(F) Representative immunofluorescence images of PPARγ-labeled FAPs cultured in GM and ADM ± WNT7A (200 ng/mL). Scale bar: 100 μm. Inset scale bar: 25 μm.

(G) Percentage of PPARγ$^+$ nuclei. Two-tailed unpaired t test. $^{**}p < 0.01$. $n = 4$. Dotted line: mean of GM.

et al., 2007; Longo et al., 2004; Moldes et al., 2003; Reggio et al., 2020; Ross et al., 2000). To determine if WNT7A inhibits adipogenesis of FAPs through the canonical Wnt pathway, we cultured freshly isolated FAPs in the GM for 4 days and then subsequently treated the cells in the ADM containing WNT7A (200 ng/mL) or the prototypically canonical activator WNT3A (200 ng/mL) for 4 or 48 h (Figures 2A–2C). As expected, brief 4-h treatment with WNT3A exhibited significantly increased nuclear intensity of β-CATENIN compared with both vehicle control and WNT7A conditions (Figures 2B and 2D; $p < 0.05$ vs. WNT7A, $p < 0.01$ vs. control). Similarly, WNT3A treatment significantly increased the percentage of β-CATENIN$^+$ nuclei compared with both the vehicle control and WNT7A (Figure 2E; $p < 0.05$ vs. WNT7A and control). However, FAPs treated with WNT7A did not exhibit an increased nuclear intensity of β-CATENIN after 4- and 48-h treatment compared with the vehicle control (Figures 2B–2F). WNT7A also had no effects on the percentage of β-CATENIN$^+$ nuclei after 4- and 48-h treatment (Figures 2E and 2G). Gene expression analyses of Wnt-related genes of FAPs after 2-day WNT7A treatment revealed that genes related to the canonical WNT signaling (e.g., *Lrp5*, *Lrp6*, *Axin1*, *Axin2*, *Gsk2b*, and *Ctnnb1*) were insignificantly altered (Figures S5A and S5B). These data collectively suggest that WNT7A suppresses adipogenesis of FAPs in a β-CATENIN-independent manner.

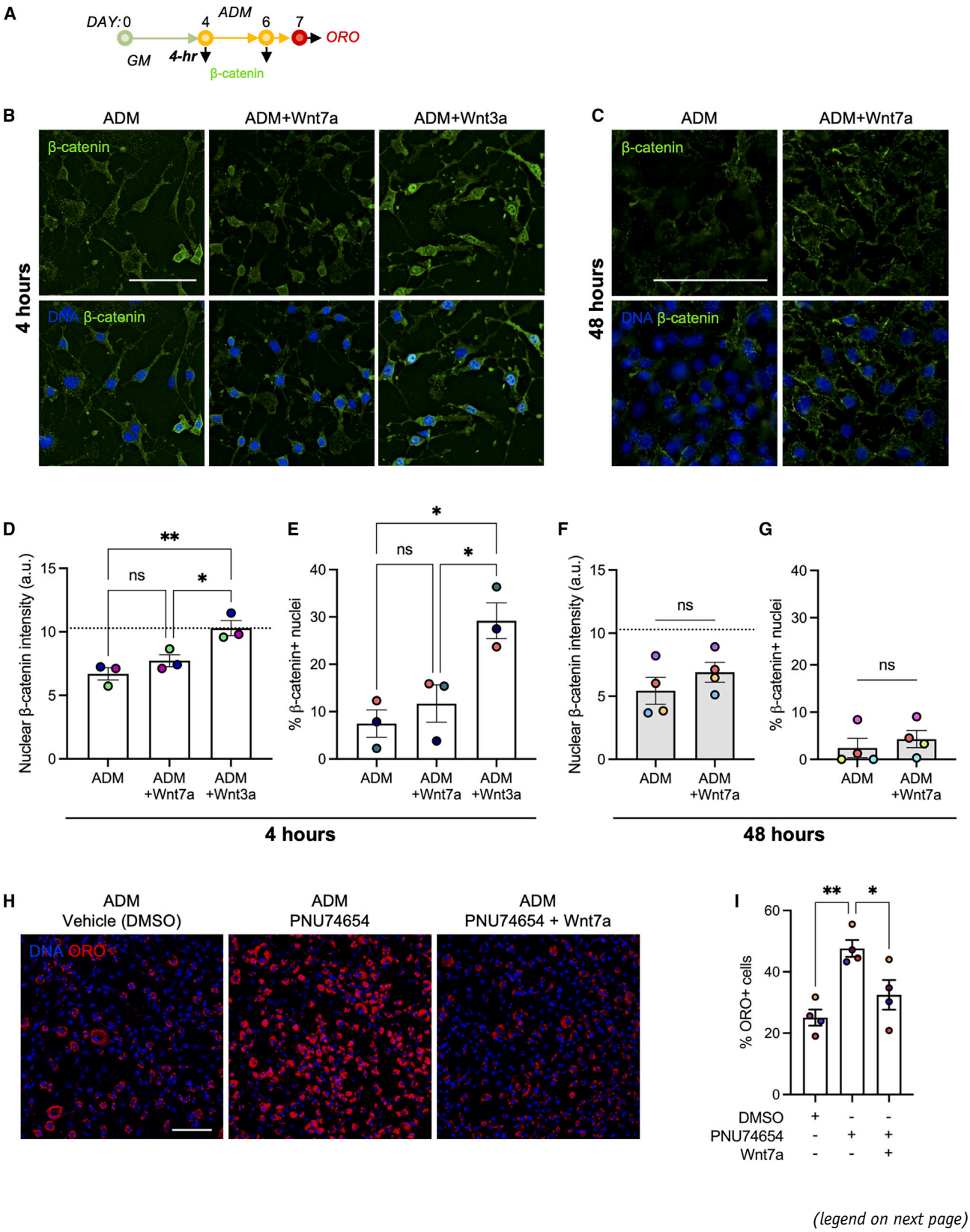

(legend on next page)

To further corroborate this finding, we next sought to inhibit the activity of β-CATENIN using a small-molecule inhibitor, PNU-74654. This inhibitor specifically prevents the binding of β-CATENIN and the T cell factor (TCF) in the nucleus. In this assay, we found that concentrations beyond 50 μM diminish FAP proliferation *in vitro*, and thus we chose to use 50 μM for the inhibition study (Figure S5C). As expected, inhibiting β-CATENIN/TCF binding with PNU-74654 significantly increased FAP adipogenesis compared with the DMSO vehicle control (Figures 2H and 2I; $p < 0.01$). However, treating FAPs with both WNT7A and PNU-74654 resulted in a marked reduction in adipogenesis compared with the PNU-74654 condition (Figures 2H and 2I; $p < 0.05$). This serves as additional evidence that WNT7A suppresses adipogenesis of FAPs in a β-CATENIN-independent manner, as WNT7A effectively reduces adipogenesis, while β-CATENIN activity remains inhibited.

WNT7A induces nuclear localization and retention of YAP

Actin cytoskeleton disassembly through Rho-ROCK signaling and subsequent cell area changes drive adipogenic differentiation of the mouse 3T3-L1 preadipocyte cell line and human stromal stem cells (Chen et al., 2018; Nobusue et al., 2014). To determine whether WNT7A reduces FAP adipogenesis through modulation of cell area and morphology, we expanded freshly isolated FAPs for 4 days and then cultured the cells in either growth and adipogenic differentiation, with or without WNT7A (Figure 3A). FAPs in the adipogenic condition (ADM) exhibited significantly reduced cell area compared with the growth condition (GM; Figures 3B and 3C; $p < 0.0001$). Note that this decrease in cell area is also accompanied by elevated levels of nuclear PPARγ (Figure 3B). In ADM, WNT7A significantly increased cell area and maximum (max) Feret diameter compared with its WNT7A-free control (Figures 3B–3D; $p < 0.0001$). In the spontaneously differentiating growth condition (GM), WNT7A also significantly increased both cell area and max Feret diameter compared with its WNT7A-free control (Figures 3B–3D; $p < 0.001$). WNT7A-treated FAPs in ADM also exhibited cell area and morphology comparable to FAPs maintained in WNT7A-free GM (Figures 3B and 3C). WNT7A treatment does not alter cell density and proliferation (Figure S4), ruling out the possibility of cell density affecting these measurements. Therefore, these results suggest that WNT7A in the adipogenic condition prevents the shrinking of cell area and maintains morphology.

YAP-1 and its paralog TAZ act as biochemical mechanotransducers that convert mechanical cues and resulting cellular changes (e.g., cell contractility and shape) into cell-specific transcriptional activities (Dupont et al., 2011). Recent evidence also suggests that YAP/TAZ also act as downstream modulators of Wnt pathways (Azzolin et al., 2012, 2014; Park et al., 2015a). Based on such evidence and our observation that WNT7A reduces FAP adipogenesis by maintaining cellular shape (Figures 3B–3D), we next questioned whether non-canonical WNT7A signaling promotes nuclear localization of YAP (Figure 3A). Nearly all freshly isolated and proliferating FAPs exhibited higher cytosolic YAP *in vitro* (Figures 3E–3G). Culturing the proliferating FAPs in WNT7A-containing GM and ADM for 4 h significantly increased the YAP nuclear-to-cytosolic ratio compared with their respective controls (Figures 3E and 3F; $p < 0.0001$). YAP nuclear localization was also

Figure 2. WNT7A reduces adipogenesis of FAPs in a β-CATENIN-independent manner

(A) Experimental timeline of β-CATENIN expression and adipogenesis study. GM, growth media; ADM, adipogenic differentiation media.

(B) Representative immunofluorescence images of β-CATENIN-labeled FAPs treated with vehicle, WNT3A (200 ng/mL), and WNT7A (200 ng/mL) for 4 h. Scale bar: 100 μm.

(C) Representative immunofluorescence images of β-CATENIN-labeled FAPs treated with vehicle and WNT7A (200 ng/mL) for 48 h. Scale bar: 100 μm.

(D) Nuclear β-CATENIN intensity analyzed at the 4-h time point. >1,000 cells analyzed per condition in an automated manner from n = 3 biological replicates. One-way ANOVA with Tukey's post-hoc analyses applied on the medians of biological donors. Mean ± SEM. *$p < 0.05$; **$p < 0.01$. n = 3. Colors represent biological replicates. Dotted line (at 10 a.u.) indicates the mean of WNT3A condition.

(E) Percentage of β-CATENIN$^+$ nuclei analyzed at the 4-h time point. One-way ANOVA with Tukey's post-hoc analyses. Mean ± SEM. *$p < 0.05$. n = 3. Colors represent biological replicates.

(F) Nuclear β-CATENIN intensity analyzed at the 48-h time point. >440 cells analyzed per condition from n = 4 biological replicates. Two-tailed unpaired t test applied on the medians of biological donors. Mean ± SEM. n = 4. Colors represent biological replicates. Dotted line (at 10 a.u.) indicates the mean of WNT3A condition from (D).

(G) Percentage of β-CATENIN$^+$ nuclei analyzed at the 48-h time point. Two-tailed unpaired t test. Mean ± SEM. n = 4. Colors represent biological replicates.

(H) Representative images of ORO-labeled cells treated with DMSO, PNU74654 (50 μM), and PNU74654 (50 μM) + WNT7A (200 ng/mL). Scale bar: 100 μm.

(I) Percentage of ORO$^+$ cells with DMSO-, PNU74654-, and PNU74654 + Wnt7a-treated conditions. One-way ANOVA with Tukey's post-hoc analyses. Mean ± SEM. *$p < 0.05$; **$p < 0.01$. n = 4. Colors represent biological replicates.

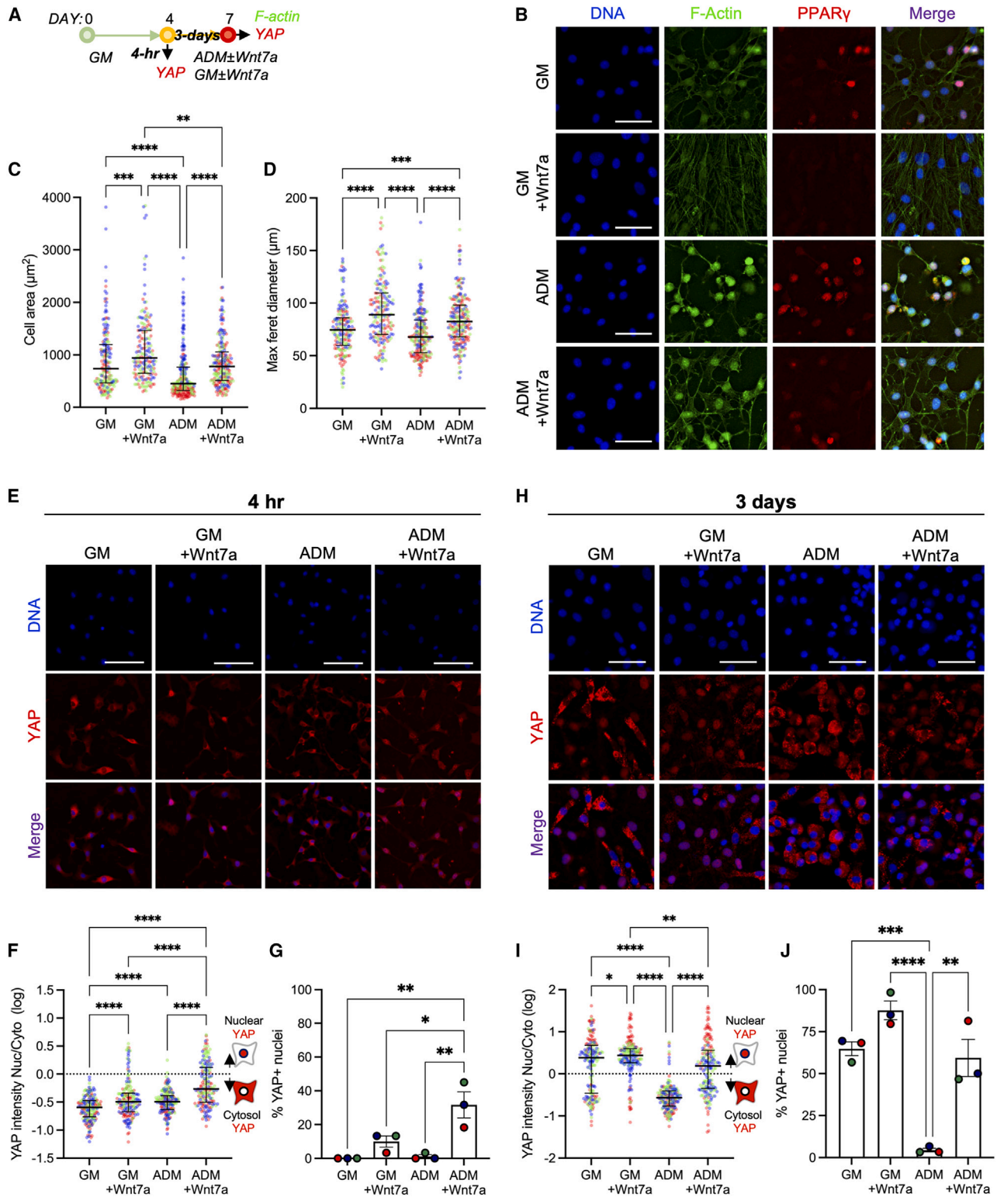

Figure 3. WNT7A induces nuclear localization and retention of YAP

(A) Experimental timeline of cell morphology and YAP quantification. GM, growth media; ADM, adipogenic differentiation media.

(B) Representative images of F-actin- and PPARγ-labeled FAPs. Scale bar: 50 μm.

(legend continued on next page)

significantly higher in ADM containing WNT7A compared with GM containing WNT7A (Figures 3E and 3F; $p < 0.0001$), suggesting context-dependent responsivity. The percentage of YAP^+ nuclei also significantly increased when FAPs were treated in ADM containing WNT7A compared with all other groups, further corroborating this finding (Figures 3E and 3G; $p < 0.05$). These results indicate that WNT7A promotes nuclear localization of YAP in proliferating FAPs *in vitro*.

To further determine if prolonged exposure of FAPs to WNT7A promotes nuclear retention of YAP, we cultured FAPs in growth (GM) and adipogenic (ADM) conditions with or without WNT7A supplementation for 3 days (Figure 3A). In GM, we observed a bimodal distribution of cells expressing nuclear and cytosolic YAP (Figures 3H and 3I), likely indicating the bifurcating lineage commitment of FAPs, but WNT7A significantly increased nuclear retention of YAP (Figures 3H and 3I; $p < 0.05$). By day 3, FAPs undergoing adipogenesis in ADM exhibited cytosolic YAP (Figures 3H–3J). In ADM, 3-day treatment with WNT7A significantly increased the nuclear retention of YAP and the percentage of YAP^+ nuclei compared with its control (Figures 3H–3J; $p < 0.01$). In addition, this WNT7A treatment also resulted in a comparable distribution of cells exhibiting nuclear and cytosolic YAP (i.e., bimodal) with GM without WNT7A (Figures 3H and 3I; $p > 0.05$). Finally, we conducted an additional experiment to determine if WNT7A-induced nuclear retention of YAP correlates with non-adipogenic FAPs. To do this, we cultured the FAPs in adipogenic conditions (ADM) with WNT7A for 3 days and co-immunolabeled the cells for both YAP and PLIN1 (Figure S6A). Approximately 85% of cells expressing nuclear YAP were $PLIN1^-$ (Figures S6B and S6C), while approximately 35% of the cells expressing nuclear YAP were $PLIN1^+$ (Figures S6B and S6C), indicating that WNT7A-induced nuclear retention of YAP negatively correlates with the adipogenic FAPs. Collectively, these data suggest that WNT7A treatment promotes nuclear localization and retention of YAP, and this likely decreases the adipogenic potential of FAPs.

WNT7A promotes YAP nuclear localization through Rho

We next asked whether WNT7A promotes nuclear localization of YAP through the alternative Wnt signaling axis involving Wnt-FZD/ROR-Rho GTPases-Lats1/2 (Park et al., 2015a; Thorup et al., 2020). In the alternative Wnt signaling, inhibition of Rho prevents Wnt-induced YAP activation. To mechanistically test this hypothesis, we pretreated FAPs in adipogenic media (ADM) containing a Rho GTPase inhibitor (purified C3 transferase; CT04) or vehicle (dH_2O) for 2 h (Figure 4A). The cells were further maintained in ADM with or without CT04 and WNT7A for an additional 4 h (Figure 4A). Here, we note that 6-h culture in ADM begins to increase the fraction of FAPs exhibiting YAP nuclear localization, contributing to an insignificant increase in the percentage of YAP^+ nuclei following WNT7A treatment (Figures 4B and 4C). Even so, WNT7A significantly increased the nuclear intensity ratio of YAP compared with the ADM control (Figure 4D; $p < 0.0001$). Rho inhibition alone did not significantly affect the nuclear intensity ratio of YAP compared with the control (Figure 4D). However, when Rho was inhibited, WNT7A failed to increase the nuclear intensity ratio of YAP (Figure 4D). The overall fraction of FAPs with nuclear or cytosolic YAP also remained unaffected when treated with WNT7A with Rho inhibited (Figure 4E). In sum, the results suggest that Rho is required for WNT7A-induced activation of YAP in FAPs.

(C) Cell area quantification. Kruskal-Wallis test with Dunn's multiple comparisons. Median ± interquartile range (IQR). **p < 0.01; ***p < 0.001; ****p < 0.0001. n = 179–219 cells analyzed from 3 biological replicates.

(D) Max Feret diameter quantification. Kruskal-Wallis test with Dunn's multiple comparisons. Median ± IQR. ***p < 0.001; ****p < 0.0001. n = 179–219 cells analyzed from 3 biological replicates. Colors represent biological replicates (C and D).

(E) Representative immunofluorescence images of YAP-labeled cells after 4-h treatment in GM ± Wnt7a (200 ng/mL) and ADM ± WNT7A (200 ng/mL). Scale bar: 100 μm.

(F) Quantification of YAP nuclear:cytosol intensity ratio at the 4-h time point. Values were log transformed. Kruskal-Wallis with Dunn's post-hoc analyses. Median ± IQR. ****p < 0.0001. n = 180 cells analyzed from 3 biological replicates. Colors represent biological replicates.

(G) Percentage of YAP^+ nuclei. One-way ANOVA with Tukey's post-hoc analyses. Mean ± SEM. *p < 0.05; **p < 0.01. n = 3. Colors represent biological replicates.

(H) Representative immunofluorescence images of YAP-labeled cells after 3-day treatment in GM ± WNT7A (200 ng/mL) and ADM ± WNT7A (200 ng/mL). Scale bars: 25 μm.

(I) Quantification of YAP nuclear:cytosol intensity ratio of the 3-day time point. Values were log transformed. Kruskal-Wallis with Dunn's post-hoc analyses. Median ± IQR. *p < 0.05; **p < 0.01; ****p < 0.0001. n = 179 cells analyzed from 3 biological replicates. Colors represent biological replicates.

(J) Percentage of YAP^+ nuclei. One-way ANOVA with Tukey's post-hoc analyses. Mean ± SEM. **p < 0.01; ***p < 0.001; ****p < 0.0001. n = 3. Colors represent biological replicates.

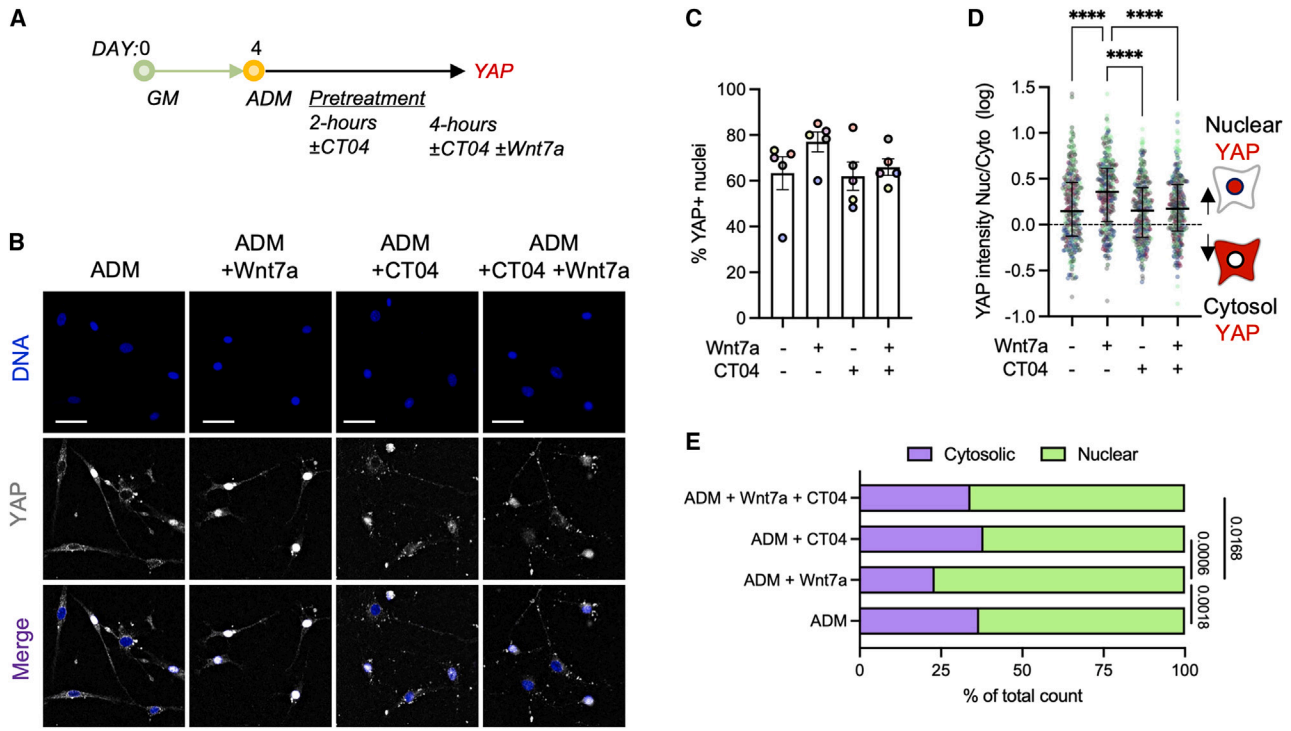

Figure 4. WNT7A activates YAP through Rho

(A) Experimental timeline of Rho inhibition study. GM, growth media; ADM, adipogenic differentiation media.

(B) Representative immunofluorescence images of YAP-labeled cells. Scale bar: 50 μm.

(C) Percentage of YAP$^+$ nuclei. One-way ANOVA with Tukey's post-hoc analyses. n = 5. Colors represent biological replicates.

(D) Quantification of YAP nuclear:cytosol intensity ratio. Values were log transformed. Kruskal-Wallis with Dunn's post-hoc analyses. Median ± IQR. ****p < 0.0001. n = 300 cells analyzed from 5 biological replicates. Colors represent biological replicates.

(E) Quantification of the cell proportions with nuclear and cytoplasmic YAP localization. Chi-squared tests. Adjusted p values for Bonferroni correction.

WNT7A promotes nuclear retention of TAZ

TAZ, a paralog of YAP-1, regulates the differentiation potential of mesenchymal stem cells by directly repressing PPARγ while activating *Runx2* genes (Hong et al., 2005). To test if WNT7A promotes TAZ nuclear localization in a similar manner to YAP, we maintained proliferating FAPs in the GM or ADM containing WNT7A for 4 h (Figure 5A). In contrast to YAP (Figures 3E–3G), most FAPs exhibited higher nuclear TAZ *in vitro* (Figures 5B–5D). WNT7A treatment in either the growth or adipogenic condition did not result in further increases in nuclear TAZ intensity (Figures 5B–5D), suggesting that WNT7A does not promote nuclear localization of TAZ in proliferating FAPs *in vitro*.

To determine if WNT7A promotes nuclear retention of TAZ in differentiating FAPs, we maintained FAPs in the ADM containing WNT7A for 24 h (Figure 5A). Nearly 80% of FAPs maintained in the ADM without WNT7A exhibited cytosolic TAZ (Figures 5E–5G), suggesting that adipogenic FAPs displace TAZ from their nucleus to cytosol. However, 24-h WNT7A treatment significantly increased nuclear retention of TAZ, quantified by both the nuclear intensity ratio of TAZ and the percentage of TAZ$^+$ nuclei (Figures 5E–5G; $p < 0.01$). In GM, FAPs homogeneously expressed nuclear TAZ at this time point, and WNT7A treatment did not further alter the TAZ nuclear localization (Figures S6D–S6F). Altogether, the results suggest that while WNT7A does not stimulate nuclear localization of TAZ, it effectively promotes nuclear retention of TAZ in differentiating FAPs in the adipogenic condition.

WNT7A suppresses fatty infiltration in skeletal muscle

We next sought to evaluate the efficacy of WNT7A in suppressing intramuscular fatty infiltration *in vivo* using the glycerol injury model. Intramuscular injection of glycerol stimulates a robust and reproducible fatty infiltration without affecting muscle regeneration, thus serving as an excellent proof-of-concept *in vivo* model to evaluate therapeutics targeted for reducing intramuscular adipogenesis (Pisani et al., 2010). To induce injury, tibialis anterior (TA) muscles were injected with glycerol

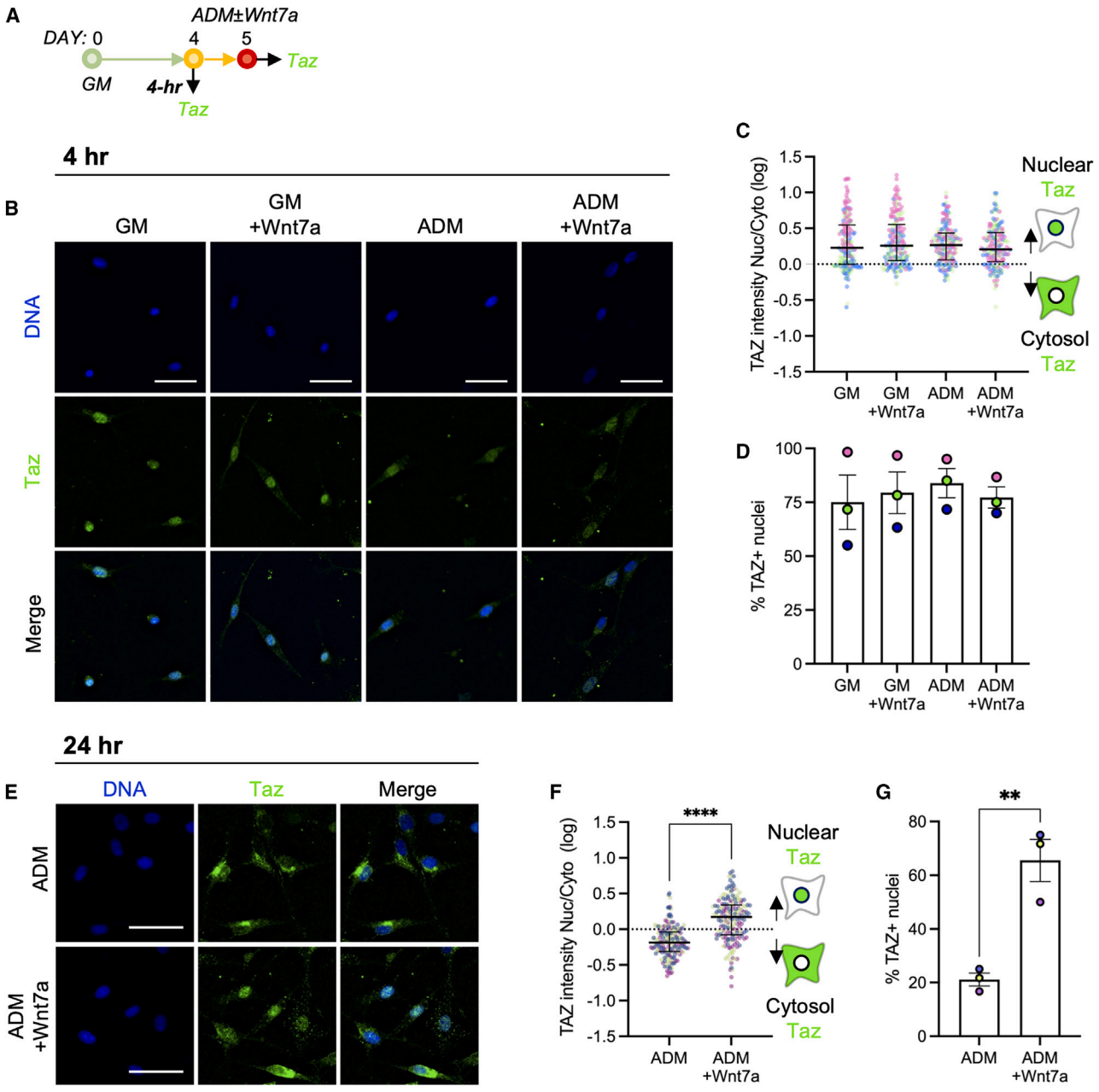

Figure 5. WNT7A promotes nuclear retention of TAZ

(A) Experimental timeline of TAZ quantification. GM, growth media; ADM, adipogenic differentiation media.

(B) Representative immunofluorescence images of TAZ-labeled cells after 4-h treatment in GM ± WNT7A (200 ng/mL) and ADM ± WNT7A (200 ng/mL). Scale bar: 50 μm.

(C) Quantification of TAZ nuclear:cytosol intensity ratio at the 4-h time point. Values were log transformed. Median ± IQR. n = 180 cells analyzed from 3 biological replicates. Colors represent biological replicates.

(D) Percentage of TAZ^+ nuclei at the 4-h time point. Mean ± SEM. n = 3. Colors represent biological replicates.

(E) Representative immunofluorescence images of TAZ-labeled cells after 24-h treatment in ADM ± WNT7A (200 ng/mL). Scale bar: 50 μm.

(F) Quantification of TAZ nuclear:cytosol intensity ratio at the 24-h time point. Values were log transformed. Two-tailed unpaired t test. Median ± IQR. ****$p < 0.0001$. n = 180 cells analyzed from 3 biological replicates. Colors represent biological replicates.

(G) Percentage of TAZ^+ nuclei at the 24-h time point. Two-tailed unpaired t test. Mean ± SEM. **$p < 0.01$. n = 3. Colors represent biological replicates.

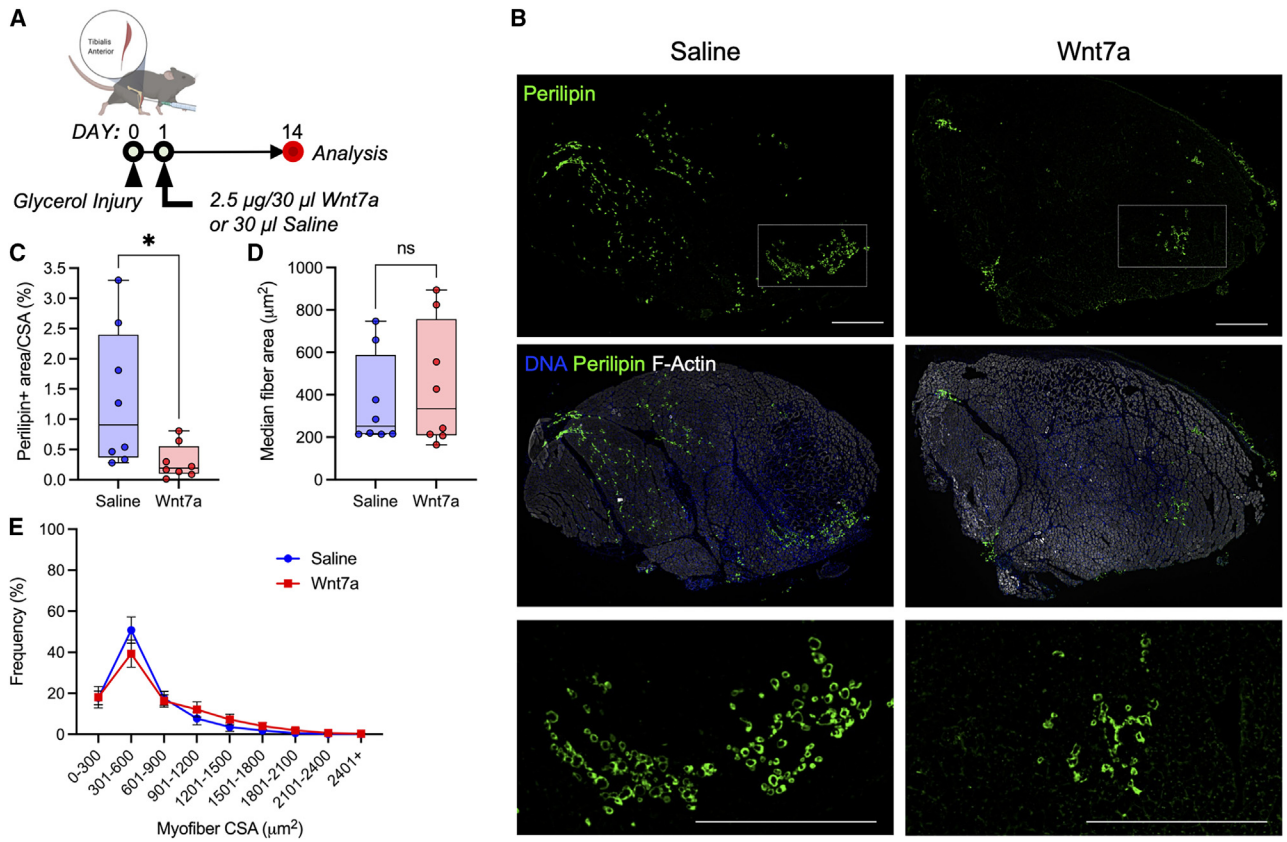

Figure 6. WNT7A suppresses fatty infiltration in skeletal muscle

(A) Experimental timeline outlining *in vivo* glycerol injection, WNT7A administration, and analyses. Created with BioRender.

(B) Representative cross-sections of glycerol-injured TA muscles treated with WNT7A or saline. Scale bars: 500 µm.

(C) Perilipin area normalized by the TA cross-sectional area. Two-tailed unpaired t test. *p = 0.027.

(D) Median fiber cross-sectional area. Two-tailed unpaired t test.

(E) Histogram of fiber cross-sectional area. Mean ± SEM.

(50% v/v). WNT7A or saline was injected into the belly of the injured TA muscles 1 day post-injury (Figure 6A). The muscles were then harvested 14 days post-injury for analyses (Figure 6A). Glycerol-injured TAs with saline treatment exhibited a severe fatty infiltration, marked by PLIN1 expression within the interstitial space (Figures 6B and S7A). However, glycerol-injured TAs with WNT7A treatment exhibited a significantly reduced PLIN1 expression (Figures 6B, 6C, and S9A; $p < 0.05$). We observed no statistically significant differences in the myofiber area distribution (Figures 6D and 6E). We also observed no qualitative and quantitative differences in fibrosis assessed by trichrome staining and polarized light imaging (Figures S7B–S7D). These data collectively show that WNT7A effectively suppresses intramuscular fatty infiltration *in vivo* without negatively impacting myogenesis or inducing fibrosis.

DISCUSSION

Persistent fatty infiltration is a chronic hallmark of skeletal muscle injuries and diseases, such as rotator cuff injuries and Duchenne muscular dystrophy (Fu et al., 2021; Li et al., 2015). WNT7A has been emerging as a potential therapeutic for muscle diseases and injuries due to its pro-regenerative effects on muscle satellite cells and myofibers (Han et al., 2019; Le Grand et al., 2009; von Maltzahn et al., 2011), but its effects on FAPs remain unknown. Thus, addressing the effects of WNT7A in modulating fatty infiltration and FAP function is critical for translating WNT7A as a potential therapeutic. In this study, we determined the mechanistic effect of WNT7A on adipogenesis of FAPs, which are the precursors to fatty infiltration in skeletal muscle pathology (Joe et al., 2010; Liu et al., 2016; Uezumi et al., 2010; Wosczyna et al., 2012). Our data reveal that WNT7A suppresses adipogenesis by inducing nuclear

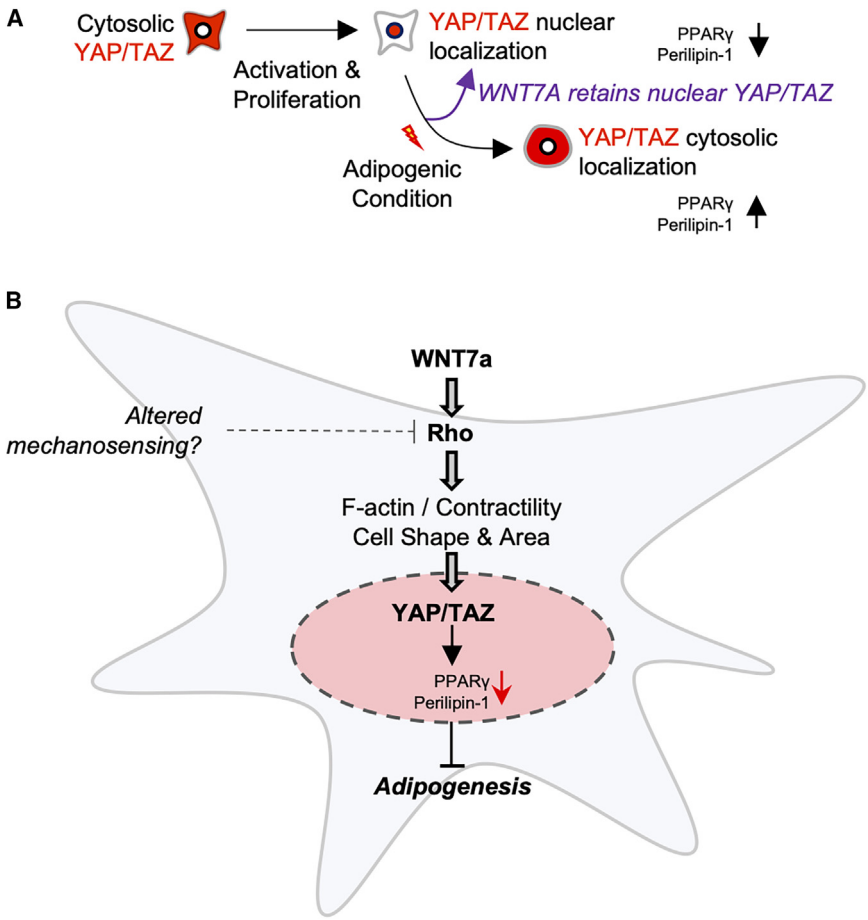

Figure 7. WNT7A retains nuclear YAP/TAZ and decreases FAP adipogenesis

(A) During adipogenesis, YAP/TAZ translocate to cytosol. WNT7A promotes nuclear retention of YAP/TAZ within the nucleus, thereby preventing FAP adipogenesis.

(B) WNT7A may rescue mechanical unloading-induced FAP adipogenesis by reinforcing YAP/TAZ activity through cell contractility-mediated mechanisms.

localization of YAP through Rho and, subsequently, by promoting nuclear retention of YAP and TAZ.

The mechanistic role of canonical Wnt signaling and β-CATENIN in suppressing adipogenesis is well established in other cell types (Bennett et al., 2002; Kang et al., 2007; Longo et al., 2004; Moldes et al., 2003; Reggio et al., 2020; Ross et al., 2000). For instance, WNT5A reduces adipogenesis of FAPs through canonical Wnt signaling (Reggio et al., 2020). Thus, we first sought to determine if WNT7A increased nuclear β-CATENIN through the canonical pathway in FAPs. WNT7A did not increase nuclear β-CATENIN in FAPs (Figures 2B–2G). Furthermore, WNT7A remained effective in reducing adipogenesis even when β-CATENIN activity was inhibited using PNU-74654 (Figures 2H and 2I), suggesting that WNT7A acts through a non-canonical pathway. We also observed that WNT7A retained a larger cell area of FAPs in adipogenic culture conditions while preventing adipogenesis (Figures 3B–3D). Based on these findings, we then asked if WNT7A acts through alternative Wnt signaling, where YAP is activated through the Wnt-FZD/Ror-Rho GTPases-Lats1/2 signaling axis independent of β-CATENIN (Park et al., 2015a). In support of our hypothesis, a brief 4-h WNT7A treatment induced nuclear localization of YAP in FAPs (Figures 3E–3G). We found that WNT7A failed to induce nuclear localization of YAP when Rho was inhibited using CT04 (Figure 4). These data suggest that WNT7A activates YAP through Rho-dependent alternative Wnt signaling in FAPs (Figure S10). These findings also raise an interesting hypothesis in which fatty infiltration that arises from skeletal muscle unloading (Kaneshige et al., 2022) may potentially be compensated through exogenous WNT7A that acts through the mechanosignaling pathway involving Rho and YAP (Figure 7). In contrast to YAP, however, we found that WNT7A does not promote TAZ nuclear localization (Figures 5B–5D). This is likely because most proliferating FAPs express nuclear TAZ (Figures 5B–5D), while YAP is localized in the cytosol (Figures 3E–3G). Nonetheless, FAPs differentiating into adipogenic lineage begin to displace both YAP and TAZ from their nuclei, and WNT7A promotes nuclear retention of YAP and TAZ. (Figures 3H–3J, 5E–5G, and 7).

How does WNT7A-induced YAP/TAZ nuclear retention inhibit PPARγ and adipogenesis of FAPs? First, published

evidence suggests that the nuclear activity of YAP/TAZ inhibits adipogenesis by repressing PPARγ in multiple cell types (Deng et al., 2019; El Ouarrat et al., 2020; Hong et al., 2005; Lorthongpanich et al., 2019; Pan et al., 2018). Specifically, TAZ directly represses PPARγ while activating *Runx2* genes in mesenchymal stem cells (Hong et al., 2005). The same mechanism may also be reducing the adipogenesis of FAPs when treated with WNT7A because WNT7A promotes nuclear retention of YAP/TAZ in differentiating FAPs and suppresses adipogenesis. Second, YAP/TAZ activity and TEAD-induced transcription may trigger the secretion of canonical Wnt modulators (Park et al., 2015a). As noted above, Wnt/β-CATENIN signaling is a crucial mediator of adipogenesis, where its downregulation results in the differentiation of preadipocytes into mature adipocytes (Bennett et al., 2002; Longo et al., 2004; Ross et al., 2000). In the current study, we observed that inhibiting β-CATENIN activity using PNU-74654 alone increased adipogenesis of FAPs (Figures 2H and 2I), suggesting that β-CATENIN indeed plays a role in modulating adipogenesis. However, WNT7A did not promote nuclear localization of β-CATENIN in FAPs after 4- and 48-h treatment (Figures 2B–2G), nor did it significantly increase expressions of genes related to the canonical Wnt signaling (Figures S5A and S5B), suggesting that WNT7A-induced YAP/TAZ activity does not significantly upregulate the canonical Wnt signaling. Interestingly, *Wisp1*, which directly binds and represses PPARγ to inhibit adipogenesis (Ferrand et al., 2017), was significantly upregulated with WNT7A treatment.

WNT7A promotes nuclear localization of YAP through Rho, increases nuclear retention of YAP/TAZ in differentiating FAPs, and suppresses adipogenesis, but it is currently unclear which receptors expressed by FAPs are binding to WNT7A to elicit the observed downstream effects. WNT7A binds to FZD7 to promote satellite cell expansion and myotube hypertrophy (Le Grand et al., 2009; von Maltzahn et al., 2011), and because FZD7 is also expressed by the FAPs (Reggio et al., 2020), it is also likely that WNT7A promotes nuclear localization and retention through FZD7. Furthermore, based on the published prior studies that describe the mechanistic link between the Wnt and Hippo signaling pathways (Park et al., 2015a; Thorup et al., 2020), we speculate that WNT7A acts by binding to the Frizzled and tyrosine kinase-like orphan receptor-1/2 (ROR1/2) complexes. In this non-canonical pathway, the binding of Wnt ligands to Frizzled and ROR1/2 co-receptors increases Rho activity that subsequently inhibits Lats1/2 (Park et al., 2015a; Thorup et al., 2020). Interestingly, querying the publicly available single-nucleus skeletal muscle gene expression database (https://research.cchmc.org/myoatlas/) (Petrany et al., 2020) revealed that ROR1 is highly expressed by murine FAPs at all ages (postnatal day 3 through 30 months of age). Whether WNT7A binds the ROR1 co-receptor to promote YAP/TAZ nuclear localization and retention remains to be addressed in future studies.

While *in vivo* administration of WNT7A to the glycerol-injured TA significantly suppressed fatty infiltration, WNT7A did not improve muscle regeneration. This is in contrast to previous findings that demonstrated that WNT7A enhances muscle regeneration (Han et al., 2019; Le Grand et al., 2009; von Maltzahn et al., 2011). The difference between the current and prior findings on the effect of WNT7A on muscle regeneration is likely due to different modes of injury used: cardiotoxin vs. glycerol. While cardiotoxin and glycerol injections induce comparable levels of muscle damage, the regeneration rate following glycerol-induced injury is dampened compared with cardiotoxin-induced injury (Lukjanenko et al., 2013). Furthermore, ectopic fatty infiltration formed following glycerol-induced injury is significantly higher compared with cardiotoxin injection, which may further reduce WNT7A-induced regeneration and hypertrophy (Lukjanenko et al., 2013). Finally, glycerol-induced injury also elicits increased gene expression of anti-inflammatory cytokines compared with cardiotoxin (Lukjanenko et al., 2013). These differences, along with the single time point assessed in the current study, likely contribute to an insignificant improvement in regeneration.

The current study has its limitations. Our current *in vitro* experiments applied a narrow time frame in which these FAPs are either spontaneously differentiating or induced to differentiate in cell culture settings. Future investigations will validate the observed mechanisms using clinically relevant *in vivo* injury and disease models. The cellular identity of the WNT7A-treated FAPs *in vivo* is also an important consideration. To further develop WNT7A as therapeutic, potential cross-talk between FAPs and other cell populations should be considered *in vivo* in a context-dependent manner as well. Functional measures, including muscle contractile force, mouse gait, and fibrosis, should also be considered to comprehensively evaluate WNT7A as a potential therapeutic. Ultimately, an effective delivery method using biomaterials such as engineered hydrogels should be tested to show the effectiveness and efficiency of WNT7A release on therapeutic models.

In conclusion, we identified that WNT7A suppresses adipogenesis of FAPs by inducing nuclear localization of YAP through Rho in a β-CATENIN-independent manner and by promoting nuclear retention of YAP and TAZ. Our data provide insight into applying WNT7A as a potential therapeutic for mitigating intramuscular fatty infiltration in various skeletal muscle pathologies.

EXPERIMENTAL PROCEDURES

Resource availability

Corresponding author

Request for resources, reagents, and protocols should be addressed to the corresponding author, Woojin M. Han, PhD (woojin.han@mssm.edu).

Materials availability

This study did not generate unique materials.

Data and code availability

All data needed to evaluate the conclusion of the paper are present in the paper or the supplemental information.

Mice

All animal procedures were conducted under the approved protocol by the Icahn School of Medicine at Mount Sinai Institutional Animal Care and Use Committee. Mice were housed and maintained in the Center for Comparative Medicine and Surgery Facility of the Icahn School of Medicine at Mount Sinai. C57BL/6J mice were acquired from the Jackson Laboratory (stock #000664). Both male and female mice were used in a randomized manner.

Glycerol injuries and WNT7A administration

2-month-old mice were anesthetized with isoflurane. 50 μL 50% glycerol in saline was intramuscularly injected into both TA muscles. After 24 h, 2.5 μg/30 μL recombinant human WNT7A (PeproTech) and 30 μL saline were injected into the TA muscles in a randomized manner. Buprenorphine shots were subcutaneously administered every 12 h at the onset of the procedure for 3 days. Mice were sacrificed on day 14 for histological analyses.

Isolation of FAPs

Primary FAPs were isolated from 4- to 6-week-old mice by magnetic-activated cell sorting (MACS) as described previously (Marinkovic et al., 2019). Mouse hindlimb muscles were dissected and incubated in digestion media (2.5 U/mL Dispase II, Thermo Fisher Scientific, and 0.2% w/v collagenase type II, Worthington, in DMEM) on a shaking incubator at 37°C for 1.5 h. Deactivation media (20% FBS in Ham's F-10; Gibco) was added to inactivate the reaction. The muscle digest was filtered through a 70-μm cell strainer and then centrifuged (300 × g, 5 min, 4°C). Cell pellets were resuspended in Staining Buffer (0.5% bovine serum albumin and 2 mM EDTA in PBS) and filtered through a 35-μm cell strainer. Cells were incubated with biotin anti-mouse CD31 (BioLegend, cat. no. 102503; 1:150), Biotin anti-mouse CD45 (BioLegend, cat. no. 103103; 1:150), and biotin anti-integrin α7 (Miltenyi, cat. no. 130-101-979; 1:10) antibodies at 4°C for 45 min. Cells were pelleted through centrifugation and incubated with 10 μL streptavidin beads (1:30) at 4°C for 15 min. Labeled cells were passed through an LD column (Miltenyi) for negative selection. The remaining cells were incubated with biotin anti-mouse Ly-6A/E (SCA-1) antibody (BioLegend, cat. no. 122504; 1:75) at 4°C for 20 min and then 10 μL streptavidin beads (1:30) at 4°C for 10 min. Cells were then passed through an LS column (Miltenyi) and enriched for SCA-1$^+$ cells. Cells were filtered through a 35-μm cell strainer once more before cell seeding.

FAP culture and differentiation

Isolated FAPs were seeded at ∼10,000 cells per 1 cm^2 well in GM (10% FBS and 1× penicillin-streptomycin in DMEM) containing 2.5 ng/mL bFGF (Peprotech) on laminin- (Gibco; 10 μg/mL) and collagen I-coated (Thermo Fisher Scientific; 5 μg/mL) plates. Cultures were maintained at 37°C and 5% CO_2 levels. Adipogenic differentiation was performed by incubating the FAPs in ADM: 0.5 mM 3-isobutyl-1-methylxanthine (Millipore Sigma), 0.25 μM dexamethasone (Millipore Sigma), and 1 μg/mL insulin (Millipore Sigma) in GM and adipogenic maintenance medium: 1 μg/mL insulin in GM. Fibrogenic differentiation was performed by incubating the FAPs in fibrogenic medium: 10 ng/mL TGF-β1 (PeproTech) in GM.

In vitro assays and reagents

Unless otherwise noted, recombinant human WNT7A (PeproTech; 200 ng/mL; vehicle: dH_2O) was added to the culture media. To inhibit β-CATENIN binding to TCF4, PNU-74654 (Cayman Chemicals; 50 μM; vehicle: DMSO) was added to the media for 3 days in ADM. To inhibit Rho, CT04 (cytoskeleton; 2 μg/mL; vehicle: dH_2O) was added to the media for 2 h as pretreatment plus an additional 4 h with or without WNT7A. The live/dead staining assay was performed using the LIVE/DEAD Cell Imaging Kit (Thermo Fisher Scientific) following the manufacturer's instructions. Cell-permeant Calcein AM was used as the live cell indicator, and cell-impermeant BOBO-3 iodide nucleic acid dye was used as the dead cell indicator.

Real-time quantitative PCR

mRNA was extracted from cells using the RNeasy Plus Microkit (Qiagen, cat. no. 74034), and cDNA was prepared using the RT2 First Strand Kit (Qiagen, cat. no. 330401). RT2 SYBR Green qPCR Master Mix (Qiagen, cat. no. 330504) and RT2 Profiler PCR Array Mouse WNT Signaling Pathway ABI 7900HT Standard Block plates (Qiagen, cat. No. PAMM-043ZA) were used for qPCR.

Immunocytochemistry staining

Cells were fixed with 4% paraformaldehyde (PFA) for 20 min at room temperature. Samples were washed three times with 1× PBS and incubated in blocking/permeabilization buffer (5.0% goat serum, 2.0% bovine serum albumin, 0.5% Triton X-100 in PBS) overnight at 4°C. For PDGFRα staining, blocking/permeabilization buffer without the goat serum (2.0% bovine serum albumin, 0.5% Triton X-100 in PBS) was used. The following primary and secondary antibodies were used for immunocytochemistry in this study: anti-PLIN (Abcam; ab3526; 1:200); anti- αSMA (Abcam; ab7817; 1:200); anti-YAP (Santa Cruz Biotechnology; sc101199; 1:200); anti-TAZ (Cell Signaling Technology; 83669S; 1:100); anti-PPARγ (Santa Cruz Biotechnology; sc7273; 1:200); anti-PDGFRα (R&D Systems; AF1062; 1:200); anti-β-CATENIN (Cell Signaling Technology; 8480S; 1:100); goat anti-rabbit Alexa 488 (Thermo Fisher Scientific; A11008; 1:500); goat anti-mouse Alexa Fluor 546 (Thermo Fisher Scientific; A11003; 1:500); goat anti-mouse Alexa 488 (Thermo Fisher Scientific; PIA32723; 1:500); and goat anti-rabbit Alexa 647 (Thermo Fisher Scientific; PIA32733; 1:500). Hoechst 33342 (Thermo Fisher Scientific; 1:1,000) and Phalloidin-iFluor 488 (Cayman Chemicals; 1:1,000) were used to stain nuclei and F-actin, respectively.

Oil Red O (ORO) staining

Cells were fixed with 4% PFA for 20 min at room temperature. Samples were washed three times with 1× PBS and incubated in blocking/permeabilization buffer (5% goat serum, 2% bovine serum albumin, 0.5% Triton X-100 in PBS) overnight at 4°C. Cells were incubated in isopropanol (60%) for 5 min and then incubated in ORO for 20 min. Cells were washed five times with 1× PBS and then counterstained with Hoechst 33342 (Thermo Fisher Scientific; 1:1,000).

Histology and immunohistochemistry

Detailed protocol is provided in the supplemental experimental procedures.

Imaging and image analysis

Images were taken on a Leica Microsystems THUNDER DMi8 microscope using LAS-X software for processing. Detailed image analysis protocol is provided in the supplemental experimental procedures.

Statistical analysis

Statistical analyses were performed using GraphPad Prism software. Normality was determined using the Shapiro-Wilk test and Q-Q plot. To test statistical significance, two-tailed t test, one-way analysis of variance (ANOVA) with Tukey's post-hoc analysis, two-way ANOVA with Bonferroni post-hoc analysis, and Kruskal-Wallis test with Dunn's multiple comparisons were performed depending on data normality and the number of comparisons. $p < 0.05$ was considered statistically significant. All experiments and studies had at least three biological replicates.

SUPPLEMENTAL INFORMATION

Supplemental information can be found online at https://doi.org/10.1016/j.stemcr.2023.03.001.

AUTHOR CONTRIBUTIONS

C.F., B.C.-Y., and W.M.H. conceived and designed the studies. C.F., B.C.-Y., G.P., M.G.-S., D.L., and W.M.H. conducted experiments and analyzed data. C.F., B.C.-Y., G.P., and W.M.H. wrote and revised this manuscript.

ACKNOWLEDGMENTS

We thank Nada Marjanovic (Sinai qPCR Core) for her work on the qPCR and gene expression analysis. This study was supported by the Department of Orthopedics at the Icahn School of Medicine at Mount Sinai to W.M.H. and by the National Institute of Arthritis and Musculoskeletal and Skin Diseases of the National Institutes of Health under award number R01AR080616. The content is solely the responsibility of the authors and does not necessarily represent the official views of the National Institutes of Health.

CONFLICT OF INTERESTS

The authors declare no competing interests.

Received: June 30, 2022
Revised: February 28, 2023
Accepted: March 1, 2023
Published: March 30, 2023

REFERENCES

Azzolin, L., Zanconato, F., Bresolin, S., Forcato, M., Basso, G., Bicciato, S., Cordenonsi, M., and Piccolo, S. (2012). Role of TAZ as mediator of Wnt signaling. Cell *151*, 1443–1456. https://doi.org/10.1016/j.cell.2012.11.027.

Azzolin, L., Panciera, T., Soligo, S., Enzo, E., Bicciato, S., Dupont, S., Bresolin, S., Frasson, C., Basso, G., Guzzardo, V., et al. (2014). YAP/TAZ incorporation in the β-catenin destruction complex orchestrates the Wnt response. Cell *158*, 157–170. https://doi.org/10.1016/j.cell.2014.06.013.

Bennett, C.N., Ross, S.E., Longo, K.A., Bajnok, L., Hemati, N., Johnson, K.W., Harrison, S.D., and MacDougald, O.A. (2002). Regulation of Wnt signaling during adipogenesis. J. Biol. Chem. *277*, 30998–31004. https://doi.org/10.1074/jbc.M204527200.

Burkhart, K., Allaire, B., and Bouxsein, M.L. (2019). Negative effects of long-duration spaceflight on paraspinal muscle morphology. Spine *44*, 879–886. https://doi.org/10.1097/BRS.0000000000002959.

Butterfield, T.A., Best, T.M., and Merrick, M.A. (2006). The dual roles of neutrophils and macrophages in inflammation: a critical balance between tissue damage and repair. J. Athl. Train. *41*, 457–465.

Chen, L., Hu, H., Qiu, W., Shi, K., and Kassem, M. (2018). Actin depolymerization enhances adipogenic differentiation in human stromal stem cells. Stem Cell Res. *29*, 76–83. https://doi.org/10.1016/j.scr.2018.03.010.

Deng, K., Ren, C., Fan, Y., Pang, J., Zhang, G., Zhang, Y., You, P., and Wang, F. (2019). YAP1 regulates PPARG and RXR alpha expression to affect the proliferation and differentiation of ovine preadipocyte. J. Cell. Biochem. *120*, 19578–19589. https://doi.org/10.1002/jcb.29265.

Dupont, S., Morsut, L., Aragona, M., Enzo, E., Giulitti, S., Cordenonsi, M., Zanconato, F., Le Digabel, J., Forcato, M., Bicciato, S., et al. (2011). Role of YAP/TAZ in mechanotransduction. Nature *474*, 179–183. https://doi.org/10.1038/nature10137.

El Ouarrat, D., Isaac, R., Lee, Y.S., Oh, D.Y., Wollam, J., Lackey, D., Riopel, M., Bandyopadhyay, G., Seo, J.B., Sampath-Kumar, R., and Olefsky, J.M. (2020). TAZ is a negative regulator of PPARγ activity in adipocytes and TAZ deletion improves insulin sensitivity and glucose tolerance. Cell Metabol. *31*, 162–173.e5. https://doi.org/10.1016/j.cmet.2019.10.003.

Ferrand, N., Béreziat, V., Moldes, M., Zaoui, M., Larsen, A.K., and Sabbah, M. (2017). WISP1/CCN4 inhibits adipocyte differentiation through repression of PPARγ activity. Sci. Rep. *7*, 1749. https://doi.org/10.1038/s41598-017-01866-2.

Fu, C., Huang, A.H., Galatz, L.M., and Han, W.M. (2021). Cellular and molecular modulation of rotator cuff muscle pathophysiology. J. Orthop. Res. *39*, 2310–2322. https://doi.org/10.1002/jor.25179.

Gladstone, J.N., Bishop, J.Y., Lo, I.K.Y., and Flatow, E.L. (2007). Fatty infiltration and atrophy of the rotator cuff do not improve after rotator cuff repair and correlate with poor functional outcome. Am. J. Sports Med. *35*, 719–728. https://doi.org/10.1177/0363546506297539.

Goffin, J.M., Pittet, P., Csucs, G., Lussi, J.W., Meister, J.-J., and Hinz, B. (2006). Focal adhesion size controls tension-dependent recruitment of alpha-smooth muscle actin to stress fibers. J. Cell Biol. *172*, 259–268. https://doi.org/10.1083/jcb.200506179.

Han, W.M., Mohiuddin, M., Anderson, S.E., García, A.J., and Jang, Y.C. (2019). Co-delivery of Wnt7a and muscle stem cells using synthetic bioadhesive hydrogel enhances murine muscle regeneration and cell migration during engraftment. Acta Biomater. *94*, 243–252. https://doi.org/10.1016/j.actbio.2019.06.025.

Heredia, J.E., Mukundan, L., Chen, F.M., Mueller, A.A., Deo, R.C., Locksley, R.M., Rando, T.A., and Chawla, A. (2013). Type 2 innate signals stimulate fibro/adipogenic progenitors to facilitate muscle regeneration. Cell *153*, 376–388. https://doi.org/10.1016/j.cell.2013.02.053.

Hinz, B. (2007). Formation and function of the myofibroblast during tissue repair. J. Invest. Dermatol. *127*, 526–537. https://doi.org/10.1038/sj.jid.5700613.

Hong, J.-H., Hwang, E.S., McManus, M.T., Amsterdam, A., Tian, Y., Kalmukova, R., Mueller, E., Benjamin, T., Spiegelman, B.M., Sharp, P.A., et al. (2005). TAZ, a transcriptional modulator of mesenchymal stem cell differentiation. Science *309*, 1074–1078. https://doi.org/10.1126/science.1110955.

Joe, A.W.B., Yi, L., Natarajan, A., Le Grand, F., So, L., Wang, J., Rudnicki, M.A., and Rossi, F.M.V. (2010). Muscle injury activates resident fibro/adipogenic progenitors that facilitate myogenesis. Nat. Cell Biol. *12*, 153–163. https://doi.org/10.1038/ncb2015.

Kaneshige, A., Kaji, T., Zhang, L., Saito, H., Nakamura, A., Kurosawa, T., Ikemoto-Uezumi, M., Tsujikawa, K., Seno, S., Hori, M., et al. (2022). Relayed signaling between mesenchymal progenitors and muscle stem cells ensures adaptive stem cell response to increased mechanical load. Cell Stem Cell *29*, 265–280.e6. https://doi.org/10.1016/j.stem.2021.11.003.

Kang, S., Bennett, C.N., Gerin, I., Rapp, L.A., Hankenson, K.D., and Macdougald, O.A. (2007). Wnt signaling stimulates osteoblastogenesis of mesenchymal precursors by suppressing CCAAT/enhancer-binding protein alpha and peroxisome proliferator-activated receptor gamma. J. Biol. Chem. *282*, 14515–14524. https://doi.org/10.1074/jbc.M700030200.

Le Grand, F., Jones, A.E., Seale, V., Scimè, A., and Rudnicki, M.A. (2009). Wnt7a activates the planar cell polarity pathway to drive the symmetric expansion of satellite stem cells. Cell Stem Cell *4*, 535–547. https://doi.org/10.1016/j.stem.2009.03.013.

Lemos, D.R., Babaeijandaghi, F., Low, M., Chang, C.-K., Lee, S.T., Fiore, D., Zhang, R.-H., Natarajan, A., Nedospasov, S.A., and Rossi, F.M.V. (2015). Nilotinib reduces muscle fibrosis in chronic muscle injury by promoting TNF-mediated apoptosis of fibro/adipogenic progenitors. Nat. Med. *21*, 786–794. https://doi.org/10.1038/nm.3869.

Li, W., Zheng, Y., Zhang, W., Wang, Z., Xiao, J., and Yuan, Y. (2015). Progression and variation of fatty infiltration of the thigh muscles in Duchenne muscular dystrophy, a muscle magnetic resonance imaging study. Neuromuscul. Disord. *25*, 375–380. https://doi.org/10.1016/j.nmd.2015.01.003.

Liu, X., Ning, A.Y., Chang, N.C., Kim, H., Nissenson, R., Wang, L., and Feeley, B.T. (2016). Investigating the cellular origin of rotator cuff muscle fatty infiltration and fibrosis after injury. Muscles Ligaments Tendons J. *6*, 6–15. https://doi.org/10.11138/mltj/2016.6.1.006.

Longo, K.A., Wright, W.S., Kang, S., Gerin, I., Chiang, S.-H., Lucas, P.C., Opp, M.R., and MacDougald, O.A. (2004). Wnt10b inhibits development of white and brown adipose tissues. J. Biol. Chem. *279*, 35503–35509. https://doi.org/10.1074/jbc.M402937200.

Lorthongpanich, C., Thumanu, K., Tangkiettrakul, K., Jiamvoraphong, N., Laowtammathron, C., Damkham, N., U-Pratya, Y., and Issaragrisil, S. (2019). YAP as a key regulator of adipo-osteogenic differentiation in human MSCs. Stem Cell Res. Ther. *10*, 402. https://doi.org/10.1186/s13287-019-1494-4.

Lukjanenko, L., Brachat, S., Pierrel, E., Lach-Trifilieff, E., and Feige, J.N. (2013). Genomic profiling reveals that transient adipogenic activation is a hallmark of mouse models of skeletal muscle regeneration. PLoS One *8*, e71084. https://doi.org/10.1371/journal.pone.0071084.

von Maltzahn, J., Bentzinger, C.F., and Rudnicki, M.A. (2011). Wnt7a-Fzd7 signalling directly activates the Akt/mTOR anabolic growth pathway in skeletal muscle. Nat. Cell Biol. *14*, 186–191. https://doi.org/10.1038/ncb2404.

von Maltzahn, J., Renaud, J.-M., Parise, G., and Rudnicki, M.A. (2012). Wnt7a treatment ameliorates muscular dystrophy. Proc. Natl. Acad. Sci. USA *109*, 20614–20619. https://doi.org/10.1073/pnas.1215765109.

von Maltzahn, J., Zinoviev, R., Chang, N.C., Bentzinger, C.F., and Rudnicki, M.A. (2013). A truncated Wnt7a retains full biological activity in skeletal muscle. Nat. Commun. *4*, 2869. https://doi.org/10.1038/ncomms3869.

Marinkovic, M., Fuoco, C., Sacco, F., Cerquone Perpetuini, A., Giuliani, G., Micarelli, E., Pavlidou, T., Petrilli, L.L., Reggio, A., Riccio, F., et al. (2019). Fibro-adipogenic progenitors of dystrophic mice are insensitive to NOTCH regulation of adipogenesis. Life Sci. Alliance *2*, e201900437. https://doi.org/10.26508/lsa.201900437.

McNamara, K.P., Greene, K.A., Tooze, J.A., Dang, J., Khattab, K., Lenchik, L., and Weaver, A.A. (2019). Neck muscle changes following long-duration spaceflight. Front. Physiol. *10*, 1115. https://doi.org/10.3389/fphys.2019.01115.

Minagawa, H., Yamamoto, N., Abe, H., Fukuda, M., Seki, N., Kikuchi, K., Kijima, H., and Itoi, E. (2013). Prevalence of symptomatic and asymptomatic rotator cuff tears in the general population: from mass-screening in one village. J. Orthop. *10*, 8–12. https://doi.org/10.1016/j.jor.2013.01.008.

Moldes, M., Zuo, Y., Morrison, R.F., Silva, D., Park, B.-H., Liu, J., and Farmer, S.R. (2003). Peroxisome-proliferator-activated receptor gamma suppresses Wnt/beta-catenin signalling during adipogenesis. Biochem. J. *376*, 607–613. https://doi.org/10.1042/BJ20030426.

Nobusue, H., Onishi, N., Shimizu, T., Sugihara, E., Oki, Y., Sumikawa, Y., Chiyoda, T., Akashi, K., Saya, H., and Kano, K. (2014). Regulation of MKL1 via actin cytoskeleton dynamics drives

adipocyte differentiation. Nat. Commun. *5*, 3368. https://doi.org/10.1038/ncomms4368.

Pan, J.-X., Xiong, L., Zhao, K., Zeng, P., Wang, B., Tang, F.-L., Sun, D., Guo, H.-H., Yang, X., Cui, S., et al. (2018). YAP promotes osteogenesis and suppresses adipogenic differentiation by regulating β-catenin signaling. Bone Res. *6*, 18. https://doi.org/10.1038/s41413-018-0018-7.

Park, H.W., Kim, Y.C., Yu, B., Moroishi, T., Mo, J.-S., Plouffe, S.W., Meng, Z., Lin, K.C., Yu, F.-X., Alexander, C.M., et al. (2015a). Alternative Wnt signaling activates YAP/TAZ. Cell *162*, 780–794. https://doi.org/10.1016/j.cell.2015.07.013.

Park, J.S., Park, H.J., Kim, S.H., and Oh, J.H. (2015b). Prognostic factors affecting rotator cuff healing after arthroscopic repair in small to medium-sized tears. Am. J. Sports Med. *43*, 2386–2392. https://doi.org/10.1177/0363546515594449.

Petrany, M.J., Swoboda, C.O., Sun, C., Chetal, K., Chen, X., Weirauch, M.T., Salomonis, N., and Millay, D.P. (2020). Single-nucleus RNA-seq identifies transcriptional heterogeneity in multinucleated skeletal myofibers. Nat. Commun. *11*, 6374. https://doi.org/10.1038/s41467-020-20063-w.

Pisani, D.F., Bottema, C.D.K., Butori, C., Dani, C., and Dechesne, C.A. (2010). Mouse model of skeletal muscle adiposity: a glycerol treatment approach. Biochem. Biophys. Res. Commun. *396*, 767–773. https://doi.org/10.1016/j.bbrc.2010.05.021.

Reggio, A., Rosina, M., Palma, A., Cerquone Perpetuini, A., Petrilli, L.L., Gargioli, C., Fuoco, C., Micarelli, E., Giuliani, G., Cerretani, M., et al. (2020). Adipogenesis of skeletal muscle fibro/adipogenic progenitors is affected by the WNT5a/GSK3/β-catenin axis. Cell Death Differ. *27*, 2921–2941. https://doi.org/10.1038/s41418-020-0551-y.

Ross, S.E., Hemati, N., Longo, K.A., Bennett, C.N., Lucas, P.C., Erickson, R.L., and MacDougald, O.A. (2000). Inhibition of adipogenesis by Wnt signaling. Science *289*, 950–953. https://doi.org/10.1126/science.289.5481.950.

Schmidt, M., Poser, C., and von Maltzahn, J. (2020). Wnt7a counteracts cancer cachexia. Mol. Ther. Oncolytics *16*, 134–146. https://doi.org/10.1016/j.omto.2019.12.011.

Thorup, A.-S., Strachan, D., Caxaria, S., Poulet, B., Thomas, B.L., Eldridge, S.E., Nalesso, G., Whiteford, J.R., Pitzalis, C., Aigner, T., et al. (2020). ROR2 blockade as a therapy for osteoarthritis. Sci. Transl. Med. *12*, eaax3063. https://doi.org/10.1126/scitranslmed.aax3063.

Tidball, J.G., and Villalta, S.A. (2010). Regulatory interactions between muscle and the immune system during muscle regeneration. Am. J. Physiol. Regul. Integr. Comp. Physiol. *298*, R1173–R1187. https://doi.org/10.1152/ajpregu.00735.2009.

Uezumi, A., Fukada, S.i., Yamamoto, N., Takeda, S., and Tsuchida, K. (2010). Mesenchymal progenitors distinct from satellite cells contribute to ectopic fat cell formation in skeletal muscle. Nat. Cell Biol. *12*, 143–152. https://doi.org/10.1038/ncb2014.

Wosczyna, M.N., Biswas, A.A., Cogswell, C.A., and Goldhamer, D.J. (2012). Multipotent progenitors resident in the skeletal muscle interstitium exhibit robust BMP-dependent osteogenic activity and mediate heterotopic ossification. J. Bone Miner. Res. *27*, 1004–1017. https://doi.org/10.1002/jbmr.1562.

Wosczyna, M.N., Konishi, C.T., Perez Carbajal, E.E., Wang, T.T., Walsh, R.A., Gan, Q., Wagner, M.W., and Rando, T.A. (2019). Mesenchymal stromal cells are required for regeneration and homeostatic maintenance of skeletal muscle. Cell Rep. *27*, 2029–2035.e5. https://doi.org/10.1016/j.celrep.2019.04.074.

Yamamoto, A., Takagishi, K., Osawa, T., Yanagawa, T., Nakajima, D., Shitara, H., and Kobayashi, T. (2010). Prevalence and risk factors of a rotator cuff tear in the general population. J. Shoulder Elbow Surg. *19*, 116–120. https://doi.org/10.1016/j.jse.2009.04.006.

Stem Cell Reports, Volume *18*

Supplemental Information

WNT7A suppresses adipogenesis of skeletal muscle mesenchymal stem cells and fatty infiltration through the alternative Wnt-Rho-YAP/TAZ signaling axis

Chengcheng Fu, Britney Chin-Young, GaYoung Park, Mariana Guzmán-Seda, Damien Laudier, and Woojin M. Han

Supplemental Figures

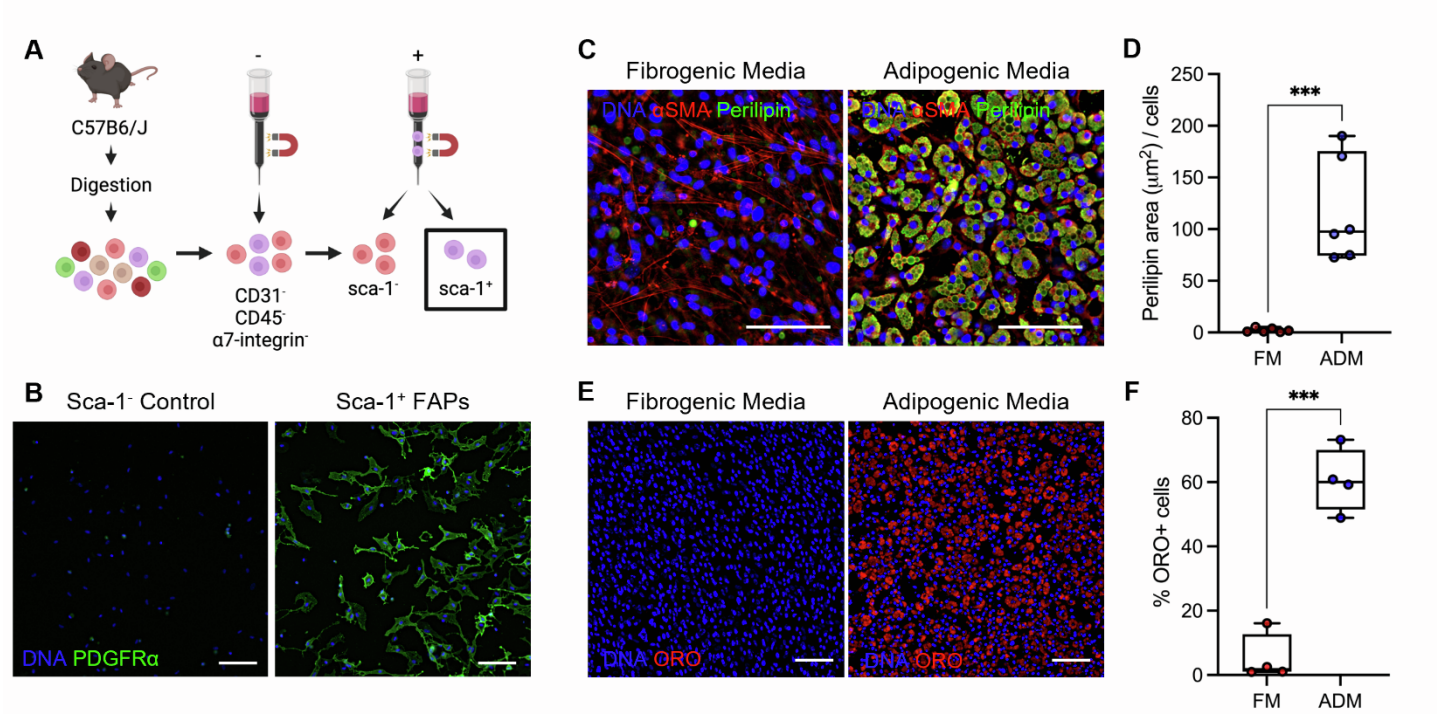

Figure S1. ***(A)*** Schematic of FAPs isolation from C57BL6/J hindlimb muscles via magnetic activated cell sorting. Created with Biorender. ***(B)*** Freshly isolated FAPs express PDGFRα. 24 hours post-seeding. Scale bar: 100 μm. ***(C)*** Representative immunofluorescence images of α-smooth muscle actin (αSMA) and perilipin-labeled FAPs differentiated in fibrogenic and adipogenic differentiation media. Scale bar: 100 μm. ***(D)*** Perilipin area normalized by cell quantity in fibrogenic (FM) and adipogenic (ADM) media. Unpaired t-test. *** $p<0.001$. n=6. ***(E)*** Representative images of Oil Red O (ORO)-labeled FAPs differentiated in fibrogenic and adipogenic differentiation media. ***(F)*** Percent ORO+ cells in fibrogenic (FM) and adipogenic (ADM) media. Unpaired t-test. *** $p<0.001$. n=4.

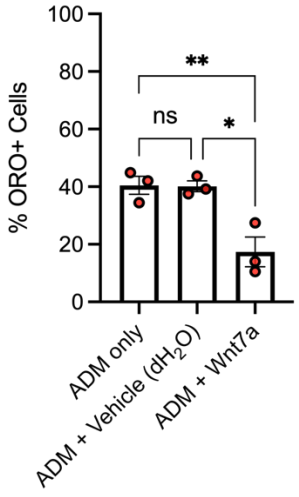

Figure S2. dH_2O vehicle in ADM (0.2% v/v) does not affect percent ORO+ cells compared to the ADM only condition. One-way ANOVA with Tukey's post-hoc analysis. * $p<0.05$; ** $p<0.01$. n=3.

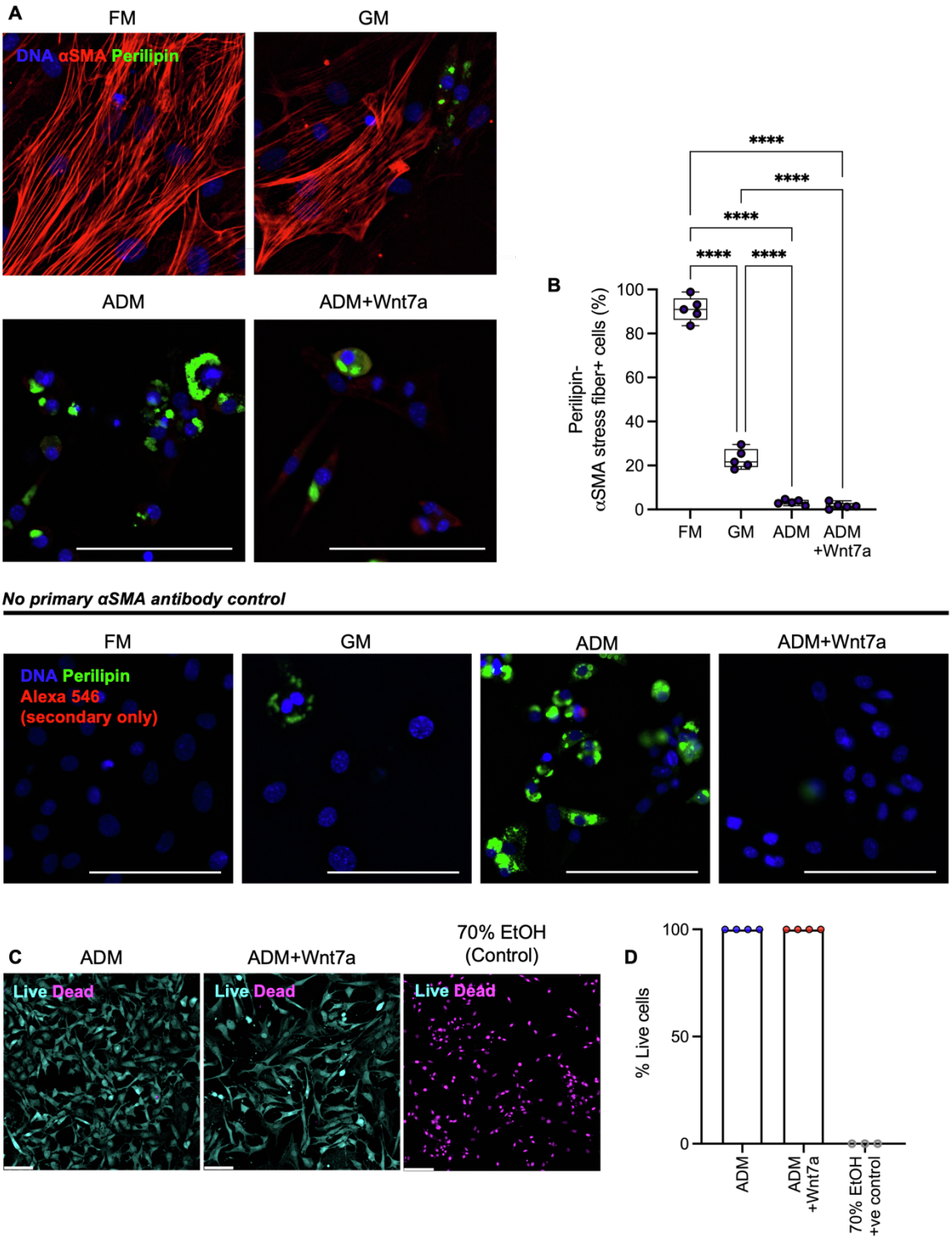

Figure S3. ***(A)*** Representative immunofluorescence images of α-smooth muscle actin (αSMA) and perilipin-labeled FAPs. Scale bar: 100 μm. ***(B)*** Quantification of % αSMA stress fiber positive cells. One-way ANOVA with Tukey's post-hoc analysis. **** p<0.0001. ***(C)*** Representative images of live-dead staining in ADM ± WNT7A conditions after 1-day treatment. A 15-min 70% EtOH treatment was used as a positive control for dead staining. Scale bar: 100 μm. ***(D)*** Quantification of % live cells show minimal cell death with WNT7A (200 ng/ml). n=4.

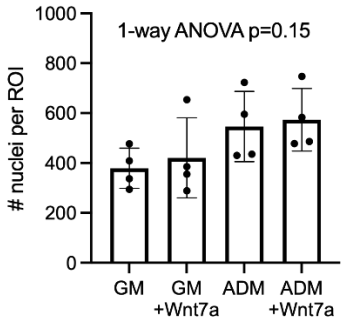

Figure S4. Number of nuclei per image determined using data from Fig. 1F. Freshly isolated FAPS were expanded for 4 days and cultured for additional 3 days in either growth and adipogenic differentiation, with or without Wnt7a.

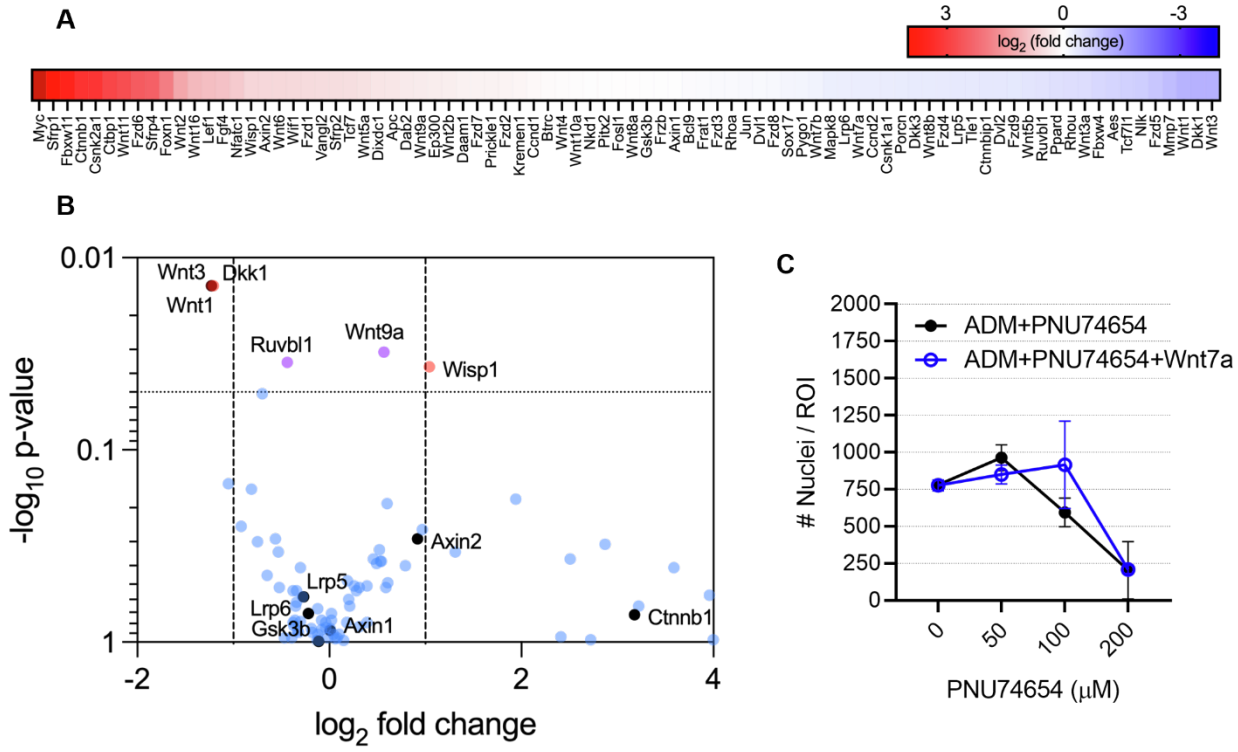

Figure S5. ***(A)*** Gene expression heat map array and ***(B)*** a volcano plot of Wnt-related genes. n=3. ***(C)*** Dose-response assay of PNU74654. Nuclei count begins to decrease around 100 μM after 5 days. n=2 per concentration.

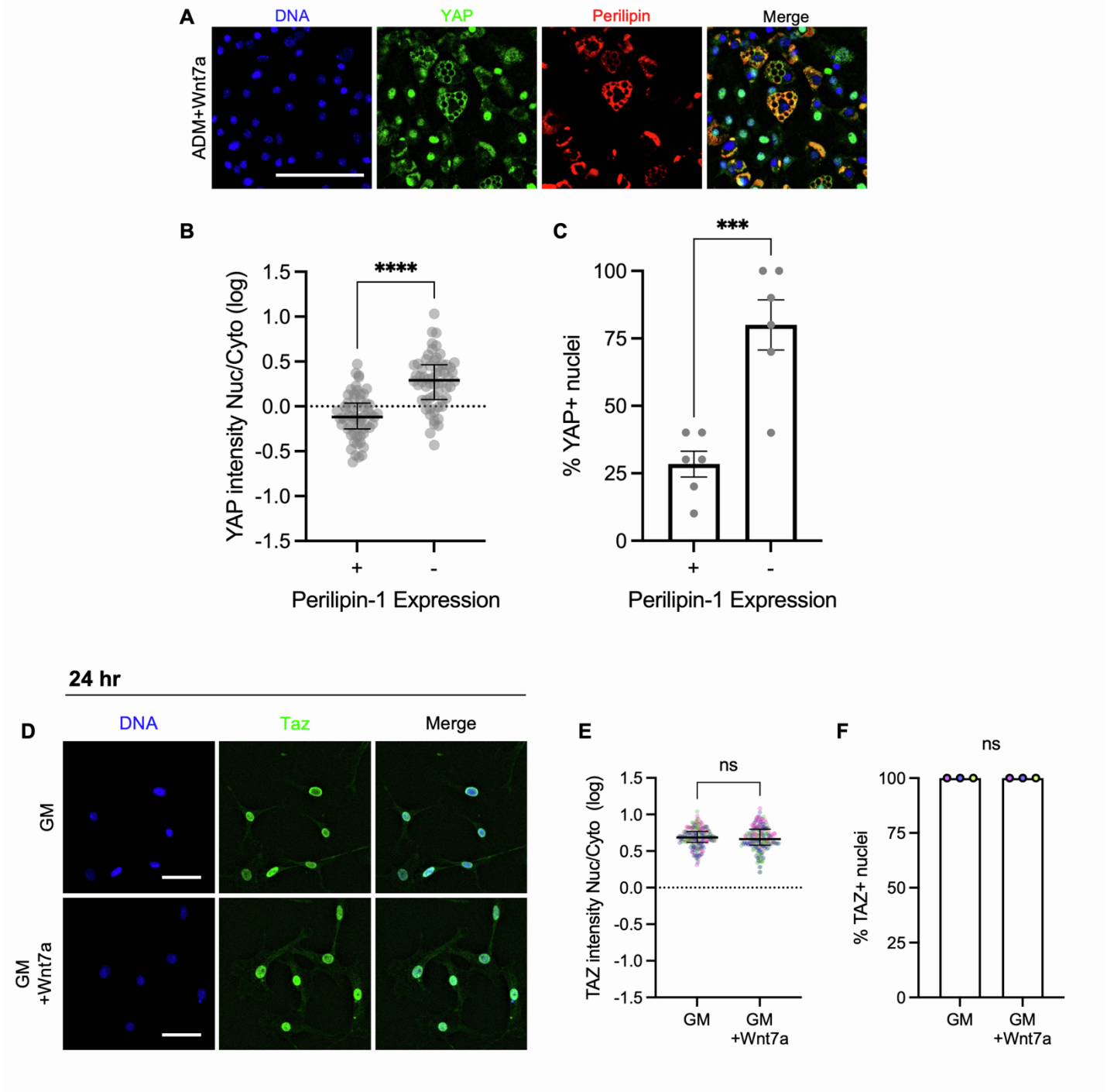

Figure S6. ***(A)*** Representative immunofluorescence images of YAP (detected with Alexa-488) and Perilipin-1 (detected with Alexa-647)-labeled cells after 3-day treatment in ADM + WNT7A (200 ng/ml). Scale bar: 100 μm. ***(B)*** Quantification of YAP nuclear:cytosol intensity ratio. Values were log-transformed. Two-tailed unpaired t-test. Median ± IQR. **** p<0.0001. 120 cells analyzed from 10 replicates. ***(C)*** Percent YAP+ nuclei. Two-tailed unpaired t-test. Mean ± SEM. **** *p*<0.0001. n=10. ***(D)*** Representative immunofluorescence images of TAZ-labeled cells after 24-hour treatment in GM ± WNT7A (200 ng/ml). Scale bar: 50 μm. ***(E)*** Quantification of TAZ nuclear:cytosol intensity ratio at the 24-hour time point. Values were log-transformed. Two-tailed unpaired t-test. Median ± IQR. **** p<0.0001. n=180 cells analyzed from 3 biological replicates. Colors represent biological replicates. ***(F)*** Percent TAZ+ nuclei at the 24-hour time point. Two-tailed unpaired t-test. n=3. Colors represent biological replicates.

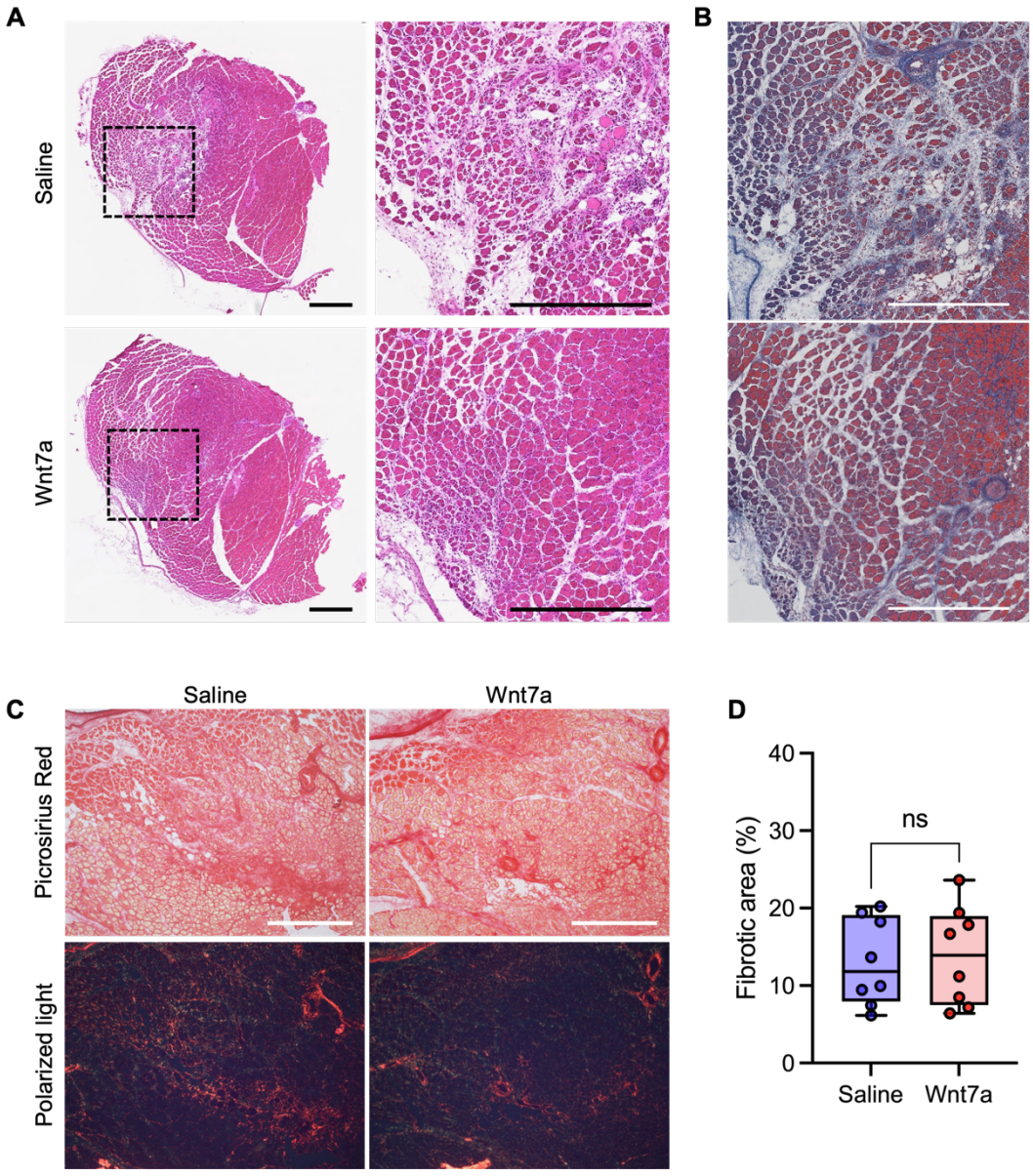

Figure S7. ***(A)*** Representative H&E staining of cross-sectioned TA muscles injected with saline ± WNT7A following glycerol-induced injury. Day 14 post-injury. Scale bar: 500 µm. ***(B)*** Representative trichrome staining of cross-sectioned TA muscles injected with saline (30 µl) ± WNT7A (2 µg/30 µl) following glycerol-induced injury. Day 14 post-injury. Scale bar: 500 µm. ***(C)*** Representative picrosirius red and polarized light images of TA muscles injected with saline ± WNT7A following glycerol-induced injury. Day 14 post-injury. Scale bar: 500 µm. ***(D)*** Quantification of the percent fibrotic area determined from polarized light. Two-tailed paired t-test.

Supplemental Experimental Procedures

Histology and Immunohistochemistry:
Hindlimbs were dissected and fixed for 1 hour at room temperature in 4% paraformaldehyde in PBS. Fixed TA muscles were dissected and frozen in liquid nitrogen-chilled isopentane. 10 μm sections were obtained from the frozen TAs using a cryotome. Tissue sections were incubated using blocking/permeabilization buffer (5.0% goat serum, 2.0% bovine serum albumin, 0.5% Triton X-100 in PBS) for 1 hour at room temperature. The following primary and secondary antibodies were used for tissue immunohistochemistry in this study: anti-perilipin (Abcam; ab3526; 1:200) and goat anti-rabbit Alexa Fluor 488 (ThermoFisher; A11008; 1:500). Hoechst 33342 (ThermoFisher; PI62249; 1:1000) and Alexa Fluor 647 Phalloidin (ThermoFisher; A22287; 1:1000) were used to stain nuclei and F-actin, respectively. Tissue sections were also processed for routine H&E, trichrome, and picrosirius red staining used for polarized light imaging.

Imaging and Image Analysis
Quantifications of perilipin area, % Oil Red O+ cells, % PPARγ+ nuclei, nuclear β-catenin intensity, in vivo perilipin+ area, and in vivo polarized light signal+ fibrotic area were performed using ImageJ in an automated manner. We describe the workflow for each measurement performed below. *Nuclei Count:* (1) Apply auto threshold (Otsu dark method) on *DNA* channel, (2) make binary, (3) apply watershed, (4) apply fill holes, (5) run analyze particle function (size 12-300 μm^2, circularity 0.3-1.0). *Perilipin area:* (1) Apply auto threshold (Otsu dark method) on *perilipin* channel, (2) convert to mask, (3) run analyze particle function (size 10-5000 μm^2). *Nuclear PPARγ count:* (1) Apply auto threshold (Otsu dark method) on *PPARγ* channel, (2) convert to mask, (3) run analyze particle function (size 45-450 μm^2). *Nuclear β-catenin intensity:* (1) make *DNA* channel binary, (2) apply watershed, (4) apply fill holes, (5) run analyze particle function (show overlay, exclude on edges, add to manager, in situ show), (6) select *β-catenin* channel, (7) run measure function from ROI Manager. *In vivo perilipin+ area:* (1) perilipin channel to 8-bit, (2) apply auto threshold (Otsu dark method), (3) set black background, (4) convert to mask, run analyze particle function (size 100-4900 μm^2). *Polarized light signal+ fibrotic area*: (1) convert polarized light image to 8-bit, (2) apply auto threshold (Otsu dark method), (3) run measure function with “area mean limit” on, (4) turn off “area mean limit” and manually outline the muscle section boundary, (5) run measure function to obtain muscle cross-sectional area and determine % fibrotic area. Myofiber areas were manually quantified using ImageJ. Cell shape metrics were manually quantified by outlining individual cells using ImageJ. The measure function was applied to determine cell area, minimum and maximum Feret’s diameter, and Feret’s angle. Note, the maximum Feret’s diameter indicates the longest distance between two points along the cell boundary, and the minimum Feret’s diameter indicates the shortest distance between two points along the cell boundary. Quantification of αSMA stress fiber+ cells was manually determined. YAP/TAZ nuclear-cytoplasmic ratios were manually quantified. Quantification of the percent YAP+ nuclei was determined by counting nuclei exhibiting Log(Nuc/Cyto) > 0.